

Provided for non-commercial research and education use.
Not for reproduction, distribution or commercial use.



This article appeared in a journal published by Elsevier. The attached copy is furnished to the author for internal non-commercial research and education use, including for instruction at the authors institution and sharing with colleagues.

Other uses, including reproduction and distribution, or selling or licensing copies, or posting to personal, institutional or third party websites are prohibited.

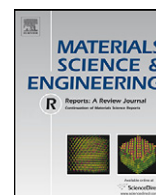
In most cases authors are permitted to post their version of the article (e.g. in Word or Tex form) to their personal website or institutional repository. Authors requiring further information regarding Elsevier's archiving and manuscript policies are encouraged to visit:

<http://www.elsevier.com/copyright>



Contents lists available at ScienceDirect

Materials Science and Engineering R

journal homepage: www.elsevier.com/locate/mser

Predictions of effective physical properties of complex multiphase materials

Moran Wang¹, Ning Pan^{*}

Nanomaterials in the Environment, Agriculture and Technology (NEAT), University of California, Davis, CA 95616, USA

ARTICLE INFO

Article history:

Available online 23 August 2008

Keywords:

Effective property
 Multiphase materials
 Complex structure
 Lattice Boltzmann
 Numerical prediction

ABSTRACT

Theoretical prediction of effective properties for multiphase material systems is very important not only to analysis and optimization of material performance, but also to new material designs. This review first examines the issues, difficulties and challenges in prediction of material behaviors by summarizing and critiquing the existing major analytical approaches dealing with material property modeling. The focus then shifts to some recent advances in numerical methodology that are able to predict more accurately and efficiently the effective physical properties of multiphase materials with complex internal microstructures. A random generation-growth algorithm is highlighted for reproducing multiphase microstructures, statistically equivalent to the actual systems, based on the geometrical and morphological information obtained from measurements and experimental estimations. Then a high-efficiency lattice Boltzmann solver for the corresponding governing equations is described which, while assuring energy conservation and the appropriate continuities at numerous interfaces in a complex system, has demonstrated its numerical power in yielding accurate solutions. Various applications are provided to validate the feasibility, effectiveness and robustness of this new methodology by comparing the predictions with existing experimental data from different transport processes, accounting for the effects due to component size, material anisotropy, internal morphology and multiphase interactions. The examples given also suggest even wider potential applicability of this methodology to other problems as long as they are governed by the similar partial differential equation(s). Thus, for given system composition and structure, this numerical methodology is in essence a model built on sound physics principles with *prior* validity, without resorting to *ad hoc* empirical treatment. Therefore, it is useful for design and optimization of new materials, beyond just predicting and analyzing the existing ones.

© 2008 Elsevier B.V. All rights reserved.

Contents

1. Introduction	2
1.1. A preview of complex materials	2
1.2. Examples of complex materials and structures	2
1.3. Effective properties of complex materials	3
1.4. Scope, objectives and structure of this review	3
2. Theoretical models	4
2.1. Existing models	4
2.1.1. Two-phase models	4
2.1.2. Multiphase cases	6
2.2. Limitations and challenges	7
3. Numerical methods	8
3.1. Structure characterization and reproduction algorithms	8
3.1.1. Structure characters of multiphase complex materials	8
3.1.2. Material structure reproduced in a computer	8
3.1.3. A random generation-growth method	9

^{*} Corresponding author. Tel.: +1 530 752 6232; fax: +1 530 752 7584.

E-mail addresses: mwang@lanl.gov (M. Wang), npan@ucdavis.edu (N. Pan).

¹ Currently working at Los Alamos National Laboratory as an Oppenheimer Fellow.

3.2.	Solutions of the governing laws	12
3.2.1.	Governing equations	12
3.2.2.	A Lattice Boltzmann solver	13
3.2.3.	Benchmarks	14
4.	Applications	15
4.1.	Different physical properties in transport	15
4.1.1.	Thermal conductivity	15
4.1.2.	Electrical conductivity	17
4.1.3.	Dielectric permittivity	17
4.1.4.	Elastic moduli	18
4.2.	The size effects	20
4.3.	Anisotropy effects	21
4.4.	Morphology effects	22
4.5.	Phase interaction effects	23
4.6.	Examination of the current measurement techniques	23
5.	Conclusions and perspectives	25
5.1.	Concluding remarks	25
5.2.	Some perspectives	25
5.2.1.	The local and global scale or size effects	25
5.2.2.	Nanoscale size effects and multiscale modeling	26
5.2.3.	Scale effect in temporal domain	26
5.2.4.	Other complexities and bi-modular behaviors	26
5.2.5.	Structural effects, biometrics and metamaterials	26
	Acknowledgements	27
	References	27

1. Introduction

1.1. A preview of complex materials

In the human endeavor in exploring new materials, a constant impetus is searching for better performance and new functionality. Translating this into fundamental scientific issue is to explore the connections between the raw ingredients, processing and the ultimate properties – transport, mechanical and other physical properties – of the resultant goods, instead of using the trial–error approach so that a better product can be designed before into the actual processing [1–9].

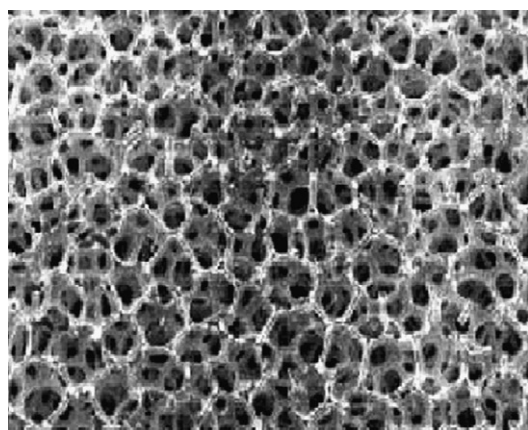
For an ideal rigid body such as those dealt with in elementary material mechanics, the material is considered as homogeneous with uniform and regular internal structure, largely resembling to the metallic materials dominant in early industrialization time. There consequently exists little difference between the properties of the material and its components—a gold brick shares virtually the same physical and chemical traits as a gold crystal. In the engineering world however, there are hardly such ideal materials. Even a gold brick has contaminations and defects in it and thus not 100% pure, and should hence be considered a mixture of the gold crystals, the contaminants (additional components), and the pores due to the defects in the molecular arrangement or the internal morphology. In other words, for a rigorous analysis of their properties, such materials have to be treated as composite systems, and the issues or influences of the structural or morphological factors have to be addressed [10]. For many engineering materials where such impurities are commonplace, it has been known long time ago that there is a rather weak correlation between the properties of the ingredients and those of the resulting products, as revealed by the pioneer works of Griffith [11] on material strength, and independently of Peirce [12] on the weakest link theorem. That is, constituents with improved quality cannot assure a better product, and the internal structure—the way the constituents are arranged in the material system is just as, if not more, important. On the other hand, the inclusion of different components into a material can be beneficial, acting as reinforcement or supplements to improve the performance of the

material—alloys and fiber reinforced composite are just such examples.

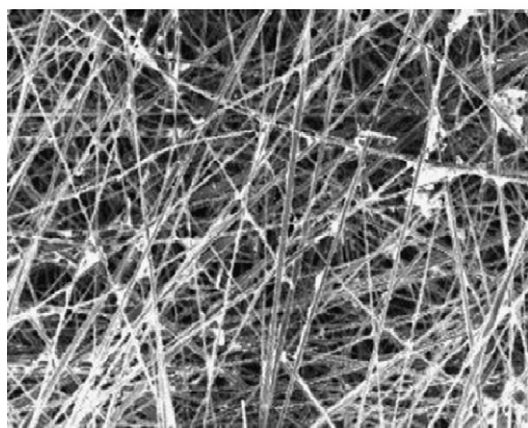
Nevertheless, analysis and prediction of behaviors of composites are in general much more intricate. Once mixed together, the components of different types will more or less interact with each other and the properties at the interfacial region will exhibit a transition from one component to the other [13–16]. Such effects usually turn even more complicated when the components are at different phase states, such as in a semi-frozen soil system [17]. The multi-component, multiphase materials are increasingly used in various fields, but analysis and investigation efforts are severely lagging behind [18,19].

1.2. Examples of complex materials and structures

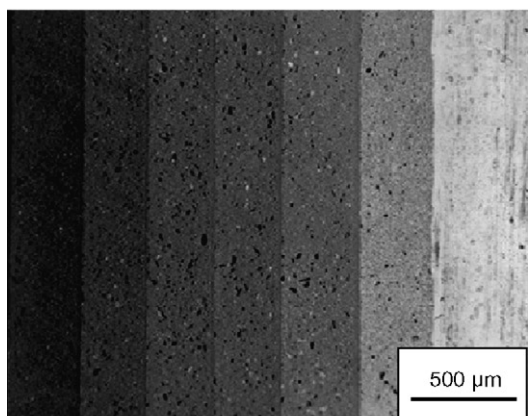
The challenges in studying complex multiphase materials come mainly from the inherent variety and randomness of their internal microstructures, and the coupling between the components of different phases. Fig. 1 shows three typical such material structures having extensive and important applications. Fig. 1a shows a cross-section of an open-cell foam material [20–25]. It has a netlike porous structure that leads, for metal-foam materials, to the interesting combination of high porosity and low density yet very high thermal and electric conductivities. Such foam materials, typically two-phase systems of solid and void, have played critical roles in advanced aircraft designs, for instance, to improve the catalytic surfaces and enhance the heat exchanger systems. The next type is a fibrous structure as shown in Fig. 1b of another solid–void mixture with the solid in a slender and oriented form, usually existing in polymeric and biomaterials [26]. For a long time, the porous transport layer (PTL) in PEM fuel cell has been thought to possess a granular porous structure; however very recent investigations have demonstrated that the PTL actually possesses a fibrous structure which exhibits quite different transport behaviors from those with granular structures [27,28]. Another example of fibrous materials is the advanced fiber reinforced composites where fibers are utilized to enhance the mechanical and thermal properties of the composites up to surprisingly high levels [29–34]. The functionally graded materials (FGM) are



(a)



(b)



(c)

Fig. 1. Three porous structures. (a) A porous open-cell foam. (b) Fibrous layer in PEM fuel cells. (c) A typical cross-section of a graded material.

another class of novel materials with spatially varied microstructures of constituent phases and gradual variation of effective properties tailored for specific performance requirements [35–38]. Fig. 1c shows the SEM micrograph of the cross-section of the $\text{Al}_2\text{O}_3/\text{Y-TZP}$ graded material. In each layer the granular alumina is dispersed in the yttria tetragonal zirconia polycrystalline (Y-TZP). Such functionally graded materials have recently gained more attention owing to their unique and tailorable properties that are suited to special applications, for instance as advanced heat-shielding materials in aerospace and electronics industries [39–41]. FGMs have also been used in actuator devices where the

materials behave better than the bimorph actuators in thermal resistance, peeling resistance and reliability owing to the absence of bonding agents [42,43]. Another application of FGMs is as a heat–electricity conversion material for design of energy conversion systems, raising the energy conversion efficiency of a nuclear or solar device by above 40% [44,45].

For systems with three or more components/phases, the microstructures or the phase distribution can become much more complicated. Even in a two-component alloy, if there are lacunae or small fractures inside, they should be treated as three-phase materials for analysis purposes [46,47]. Another often-encountered multiphase structure is that of unsaturated porous soils [48–54]; Fig. 2 illustrates two kinds of liquid phase distributions inside an unsaturated granular porous media. The gray areas represent the solid aggregates, the dark is the gas phase, and the white is the liquid phase. The interesting and complex behavior comes largely from the interactions among the different phases. Hydrophilic or hydrophobic solid surfaces will lead to, respectively, liquid films (a) or liquid droplets (b) on the solid phases. Since the thermal or electric transport properties of the liquid are drastically different from those of the gas phase, the liquid distribution will influence considerably the overall effective transport properties of the porous medium. Such problems are very critical for material optimization and design. Whereas the phase interaction effects on the material properties have not been systematically studied.

In the current wave of emerging new materials including biomaterials [55–59], multifunctional materials [60–65], nanomaterials [66–72] and energy materials [73–77], most of them are complex media in terms of both physics and structures, thus increasing the urgency for more robust theoretical and computational tools.

1.3. Effective properties of complex materials

Given the complexities of the composite systems, the concept of effective properties has become widely accepted [18,19,78–91]. Complex materials are multi-component and/or multiphase (state) systems. As such, the behaviors of the material are dictated by each and every component of different phases, that is, its overall macroscopic property is not equal to that of any single constituent, rather is a collective one contributed by all components forming the system. Therefore, the effective property is actually the equivalent property of a hypothetical simple material (homogeneous with single component and phase) which yields the same response as that of the complex one at the same given conditions and excitations [18,78–80].

Note that, however, this mapping between the complex material system and its equivalent simple material is not unique. The different components and phases in the complex system will exhibit diverse and varying behaviors under different ambient conditions and external excitations [18,79,92,93]. The system overall properties are thus the functions of these external factors as well, thus leading to different equivalent simple systems [18,78,79,92].

Research and investigation of the effective properties of complex materials are important because not only the multiphase materials have so many significant applications, but it can also shed new light on, and drive further developments, of the related mathematical, physical and engineering theories [92–103].

1.4. Scope, objectives and structure of this review

This review will summarize the existing achievements in prediction methods for the effective physical properties of complex multiphase materials. Such methods include both

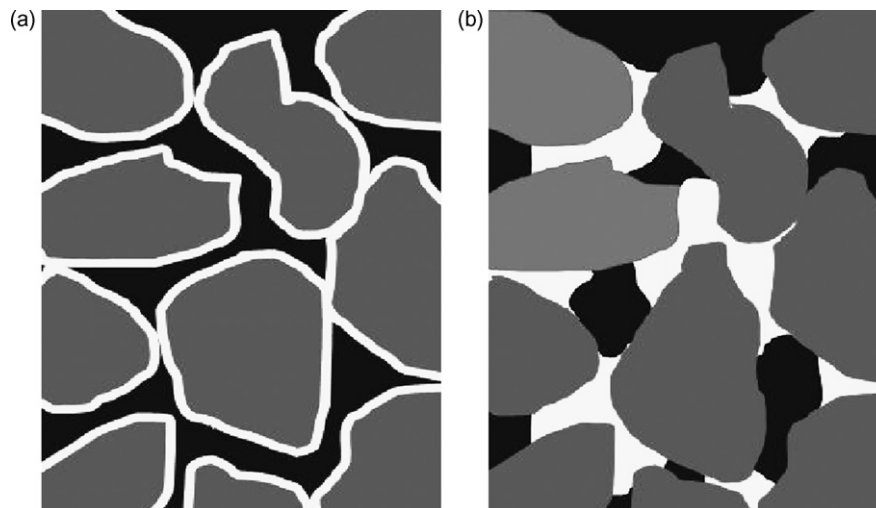


Fig. 2. Two types of three-phase granular porous media.

theoretical and the numerical ones, and the multiphase materials can have very complex microstructures and phase distributions, including various morphologies and geometries. The “effective physical properties” here are associated with three implications: (i) they are steady-state (equilibrium) macroscopic properties. Even though in some cases where nanoscale inclusions play an important role, such as in nanocomposites [85,87,104–109], only the contributions of the nanoscale inclusions to the macroscopic properties are concerned by using the *corresponding effective properties* of the inclusions. So the continuum theories are still valid for the whole system; (ii) The properties concerned are limited to pure physical properties only, and no chemical reactions are taken into account; (iii) The multiphase systems are in stable and equilibrium state with no phase change, and only very small or negligible deformations or convections, when appropriate, are allowed.

Thus, the overall objectives for this review are (1) to examine the existing models and methodologies to highlight the recent significant progresses, and to discuss the promising directions; (2) through further analysis, to bridge the microstructures and the effective physical properties for complex multiphase materials; (3) using examples to explore the inter-analogies between various properties governed by PDEs in similar form so that one can adopt the established methodologies to other untitled or unfledged questions; and (4) when possible, to connect the theoretical results with engineering applications. Through analytical predictions and numerical modeling, certain optimization approaches and design schemes for novel materials could be resulted for engineering applications, and in turn the new observations and experiences from the practice would accelerate the development of new theories and methodologies.

This review is organized as follows. The theoretical models for both two- and multiphase materials are summarized in Section 2. The significant and major models are highlighted, while the remaining limitations and challenges are detailed and analyzed. Section 3 reviews some recent progresses in numerical modeling of effective properties for multiphase media in two aspects: microstructure reproduction and numerical solution of the governing equations, with emphasis on a new mesoscopic scheme. After the numerical methods are validated by the existing experimental data of different properties in various cases, the influences of several aspects of the microstructure on the effective properties are analyzed and discussed in Section 4. Finally conclusions and potential future directions are presented in Section 5.

2. Theoretical models

A substantial number of theoretical (or analytical) models for effective physical properties have been proposed in the past of more than one hundred years [110]. Some of them have been intended for highly specific applications, while others have wider applicability. Nonetheless, most of them focus on the compositions and barely dealt with the internal geometry or microstructures beyond very simple geometrical arrangements, in spite of the critical importance of those factors on the effective properties of a complex material.

Apparently, theoretical approaches are still preferred owing to their predictive or estimative power, low cost of easy use, and reasonable accuracy for certain specific cases, especially when the microstructure can be simplified.

2.1. Existing models

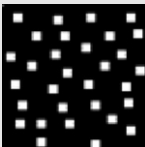
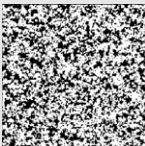
This section reviews the existing analytical models for effective physical properties of heterogeneous materials, including thermal conductivity, coefficient of thermal expansion, electric conductivity, dielectric constant (permittivity) and mechanical modulus. Although these are quite different physical properties, they share similar characteristics and general expressions of governing laws.

2.1.1. Two-phase models

For two-phase cases, the theoretical approaches include the *basic models*, *combined models*, *network models* and *theoretical bounds*.

2.1.1.1. The basic models. Most if not all of the existing analytical models for the effective physical properties in the literature are based on, or derived from, several basic models. Here we list six representative ones in Table 1, each of which has lead to a model family and played very important roles in analyzing material properties. Of them, the Parallel and Series model are the simplest for two-phase systems and are often used as benchmarks for new model validations. They often offer upper and lower bounds for many properties of two-phase heterogenous materials, as proven by Wiener for effective conductivity [111,112]. In the case of elastic modulus, they are often called the Voigt and the Reuss models, respectively [113,114]. The Parallel model also serves as the first-order approximation to the calculation of the coefficient of thermal expansion [115]. Next, the Effective Medium Theory (EMT) model tackles materials with a completely random distribution of all the

Table 1
Fundamental analytical models for effective properties of two-component materials

Model	Structure schematic ^a	Expressions ^b	Reference
Parallel model		$\lambda_e = (1 - \phi)\lambda_1 + \phi\lambda_2$	For conductivity: [111,112] For elastic modulus: [113,114] For thermal expansion coefficient: [115]
Series model		$\lambda_e = \left[\frac{1-\phi}{\lambda_1} + \frac{\phi}{\lambda_2} \right]^{-1}$	Same as parallel model
EMT model		$(1 - \phi) \frac{\lambda_1 - \lambda_e}{\lambda_1 + 2\lambda_e} + \phi \frac{\lambda_2 - \lambda_e}{\lambda_2 + 2\lambda_e} = 0$	[116–118]
Maxwell model		$\frac{\lambda_e}{\lambda_1} = 1 + \frac{3(\alpha-1)\phi}{(\alpha+2)-(\alpha-1)\phi}$	[123]
Hamilton model		$\frac{\lambda_e}{\lambda_1} = \frac{\alpha+(n-1)+(n-1)(\alpha-1)\phi}{\alpha+(n-1)+(1-\alpha)\phi}$	[133]
Reciprocity model		$\frac{\lambda_e}{\lambda_1} = \frac{1+(\sqrt{\alpha}-1)\phi}{1+(\sqrt{1/\alpha}-1)\phi}$	[119,134]

^a Assuming the heat flow is in the vertical direction.

^b Where λ_1 is the property of the continuous phase, λ_2 the property of the dispersed phase, λ_e the corresponding effective property, ϕ the volume fraction of the dispersed phase, α the property ratio ($\alpha = \lambda_2/\lambda_1$), n the shape factor of the dispersed phase.

components [111,116]. Note that the expression for EMT model is an implicit form of what proposed by Bruggeman [117,118], and it takes other forms for spherical and ellipsoidal inclusions for conductivity [119–121] and elastic moduli [122]. The Maxwell models are likely the most widely used ones in the literature, with the assumptions of a dispersion of small particles within a continuous matrix phase and the particles being far apart from each other so that the local distortions to the transport characteristics around each particle do not interfere with their neighbors [123]. The Maxwell model, which is actually also a special case of the EMT models, has led to a huge derived variations in dealing with transport phenomena, such as the well-known Maxwell–Eucken model [124], the Maxwell–Garnett model [125,126] and their sub-models [127–132]. The Hamilton–Crosser model introduces a shape factor (n) into the expression so as to deal with cases of non-spherical particle inclusions [133]. But when $n = 3$, it turns into the case of spherical particles and back to the Maxwell model, while $n = 6$ is for cylindrical particles. The

reciprocity model was based on the reciprocity theorem [134] which assumes that a microstructure of two-component remains statistically equivalent when exchanging the volume fractions of the components [135,136]. Although the idea of this model appear quite different from other models, its predictions agreed rather well with experimental data [134], and the very same expression was also derived from the Maxwell–Garnett-type approximation by including the shape distribution effects [119].

These basic models provide acceptable predictions of the effective properties for simple or simplified problems, but the applicability and the accuracy of them are clearly very limited. Three approaches have been proposed by different researchers at different cases to more or less improve their capability by (i) introducing empirical parameters to account for certain structure characteristics [137–141]; (ii) combining two or more basic models for more complex structures [142–146]; (iii) using a network formed by huge number of Parallel and Series models [147–153].

2.1.1.2. *Combined models.* Two approaches have been proposed in combining the basic models to expand the applicability. The first route is to convert a heterogeneous material into a system treatable empirically by a weighted mixture of Parallel and Series models. The effective property can then be calculated as a weighted mean of corresponding properties of the components in Parallel and Series arrangements. Harmonic, geometric and arithmetic schemes have been proposed accordingly to calculate the weighted means [143–145]. Like most empirical methods, predictions close to the experimental data have been obtained for some cases when the empirical parameters in the model can be determined. Another combinatory rule was by Wang et al. [146] based on such concepts as *structure volume fraction* and *structure composition factor* defined in their paper. The approach was demonstrated to narrow the prediction bounds for general two-phase granular materials.

2.1.1.3. *Network models.* Similar principle is applied in this approach where a complex microstructure of heterogeneous materials is decomposed into a network consisting of a set of series/parallel structural elements connected. Each element possesses properties of a pure material or even effective ones of a composite itself. The overall effective properties can then be calculated through the parallel and series laws. Comparing with other theoretical models, the network model is much more expensive because of larger number of the basic elements involved, and hence only employed for approximation of certain structures [147–153].

2.1.1.4. *Theoretical bounds.* In practice, another common way to estimate the properties of two-phase materials is to find the bounds or the ranges of the solutions, especially when the microstructures are unknown or too complicated. As stated before, the Parallel and Series models are also termed the Wiener upper and lower bounds [112,154,155]. However, for most cases these estimations are too rough, especially when contrast between the properties of the components is large. Hashin and Shtrikman [156] derived bounds based on assumed macroscopical isotropy and quasi-homogeneity of the materials, by ignoring the influence of the component shapes. The Hashin and Shtrikman (HS) bounds are always narrower, i.e., more accurate, than the Wiener bounds. For effective conductivities, the HS bounds are given as

$$\frac{\lambda_e^l}{\lambda_1} = 1 + \frac{3(\alpha - 1)(1 - \phi)}{3 + (\alpha - 1)\phi} \quad (1)$$

$$\frac{\lambda_e^u}{\lambda_1} = \alpha + \frac{3\alpha(1 - \alpha)\phi}{3\alpha + (1 - \alpha)(1 - \phi)} \quad (2)$$

where λ_e is the effective conductivity, λ_1 and λ_2 the conductivities of the two phases, with $\lambda_2 > \lambda_1$, ϕ is the volume fraction of phase 2, and $\alpha = \lambda_2/\lambda_1$; the superscript “l” represents the lower bound and “u” the upper bound.

For estimation of the elastic constants, it was proposed that [157,158]

$$K_e^u = K_2 + \frac{1 - \phi}{(1/(K_1 - K_2)) + (3\phi/(3K_2 + 4G_2))} \quad (3)$$

$$K_e^l = K_1 + \frac{\phi}{(1/(K_2 - K_1)) + (3(1 - \phi)/(3K_1 + 4G_1))} \quad (4)$$

$$G_e^u = G_2 + \frac{1 - \phi}{(1/(G_1 - G_2)) + (6\phi(K_2 + 2G_2)/5G_2(3K_2 + 4G_2))} \quad (5)$$

$$G_e^l = G_1 + \frac{\phi}{(1/(G_2 - G_1)) + (6(1 - \phi)(K_1 + 2G_1)/5G_1(3K_1 + 4G_1))} \quad (6)$$

where K represents the bulk modulus and G the shear modulus, and the phase indices are chosen such that $K_2 > K_1$. The upper and lower Hashin–Shtrikman (HS) bounds for Young's modulus of the material can be obtained as follows [157]:

$$E_{HS} = \frac{9K_e G_e}{3K_e + G_e} \quad (7)$$

where the upper and lower K_e and G_e are defined in Eqs. (3)–(6). These bounds are valid for all values of the phase stiffness ratio [113,114]. Since the corresponding bounds on the effective Poisson ratio in a form analogous to (7) were sometimes reported erroneous, the corrected HS bounds of the Poisson ratio (ν) were provided in [159]

$$\nu_e^l = \frac{3K_e^l - 2G_e^u}{6K_e^l + 2G_e^u}, \quad \nu_e^u = \frac{3K_e^u - 2G_e^l}{6K_e^u + 2G_e^l} \quad (7a)$$

in which the upper bound of K must be paired with the lower bound of G .

For the coefficient of thermal expansion, Schapery [160] developed a model for both the upper and lower bounds:

$$C_e^l = C_1 + \frac{K_2 (K_1 - K_e^u)(C_2 - C_1)}{K_e^u (K_1 - K_2)} \quad (8)$$

$$C_e^u = C_1 + \frac{K_2 (K_1 - K_e^l)(C_2 - C_1)}{K_e^l (K_1 - K_2)} \quad (9)$$

where C represents the coefficient of thermal expansion and K the corresponding bulk moduli from the HS bounds.

2.1.2. Multiphase cases

A large number of theoretical models for prediction of effective properties for multiphase materials have been developed, mainly because of the significance and interest in the effective thermal conductivity and permittivity of unsaturated soils. Roughly, the models can be classified into three major categories.

2.1.2.1. *Empirical equations.* Various empirical equations have been proposed to connect the effective property to the volume fractions of the multiple phase components, by means of fitting the experimental data [48,161–172]. For example, Cosenza et al. [164] developed the following empirical equation, valid over the solids thermal conductivity (k_s) ranging from 2 to 5 W m⁻¹ K⁻¹, porosity (ε) from 0.4 to 0.6, and the volumetric water content (θ) from 0.1 to 0.4

$$k_e = (0.8908 - 1.0959\varepsilon)k_s + (1.2236 - 0.3485\varepsilon)\theta \quad (10)$$

Such equations have proved to be useful in targeted cases, however, with many limits associated with determination of the empirical parameters absence of physical basis.

2.1.2.2. *Modified mixing models.* Based on the two-phase fundamental models, two schemes have been implemented for the multiphase case. The first is to extend the two-phase basic models directly to multiphase cases. For example, the Parallel and Series equations were adopted for rough estimations of the effective properties of multiphase materials [173]. For three-phase media, Woodside and Messmer [174] proposed the ‘quadratic parallel’ (QP) model for the effective conductivity:

$$\lambda_e = \{\lambda_1^{1/2} \phi_1 + \lambda_2^{1/2} \phi_2 + \lambda_3^{1/2} \phi_3\}^2 \quad (11)$$

where λ_i with $i = \{1, 2, 3\}$ is the conductivity of each phase and ϕ_i the corresponding volume fraction. This model appears to be applicable when $i > 3$. Various weighted average models have also been proposed for such multiphase mixtures [175].

The second route is to treat two of the multiple phases as one single phase with their own effective properties and then to mix this effective phase with another new phase, i.e., dividing a multiphase material into combination of several two-phase systems. The Maxwell models are the most suitable to developing such mixture models in general, and the Maxwell–De Looer model in particular is widely used, for it requires no geometrical parameters [176,177]. Dobson et al. [178] rewrote this model for a four-phase system into:

$$\lambda_e = \frac{3\lambda_1 + 2(\phi_2 - \phi_3)(\lambda_2 - \lambda_1) + 2\phi_3(\lambda_3 - \lambda_1) + 2(\phi_4 - \phi_2)(\lambda_4 - \lambda_1)}{3 + (\phi_2 - \phi_3)(\lambda_1/\lambda_2 - 1) + \phi_3(\lambda_1/\lambda_3 - 1) + (\phi_4 - \phi_2)(\lambda_1/\lambda_4 - 1)} \quad (12)$$

As the Maxwell models are based on the assumption that the dispersed phases are independently distributed in the continuous phase with negligible interactions with each other, these types of models fail to work properly if there exist any strong phase interactions inside the materials, unless some empirical parameters are introduced to account for those influences [178].

2.1.2.3. Analytical solutions from physical laws. Such analytical models can also be obtained from appropriate physical theories and their analytical solutions. Among those the composite spheres model proposed by Friedman [179] for effective dielectric constant (permittivity) is the most notable one. The model considers an unsaturated porous medium as an array of spherical inclusions embedded in an infinite and macroscopically homogeneous matrix and characterized by an overall effective dielectric constant ϵ_e . The inclusions are much smaller than the operated wavelength in measurements, and are in the form of spheres, each including all the three phases as depicted in Fig. 3. Under quasi-static conditions, the electrical potential field satisfies the Laplace equation, and the continuity of both the potential and the normal flux at the three inter-phases provides the boundary conditions. The derivation of the self-consistent solutions [180,181] gives the expression of the property ϵ_e in the three-phase cases as:

$$\epsilon_e = \epsilon_1 + \frac{3[(\phi_3 + \phi_2)(\epsilon_2 - \epsilon_1)(2\epsilon_2 + \epsilon_3) - \phi_3(\epsilon_2 - \epsilon_3)(2\epsilon_2 + \epsilon_1)]\epsilon_1}{(2\epsilon_1 + \epsilon_2)(2\epsilon_2 + \epsilon_3) - 2(\phi_3/\phi_3 + \phi_2)(\epsilon_2 - \epsilon_1)(\epsilon_2 - \epsilon_3) - (\phi_3 + \phi_2)(\epsilon_2 - \epsilon_1)(2\epsilon_2 + \epsilon_3) + \phi_3(\epsilon_2 - \epsilon_3)(2\epsilon_2 + \epsilon_1)} \quad (13)$$

where the volumetric fractions of the three phase, ϕ_i , is defined as, where R_i refers to the radii of the spheres

$$\phi_1 = \frac{R_1^3 - R_2^3}{R_1^3}, \quad \phi_2 = \frac{R_2^3 - R_3^3}{R_1^3}, \quad \phi_3 = \frac{R_3^3}{R_1^3} \quad (14)$$

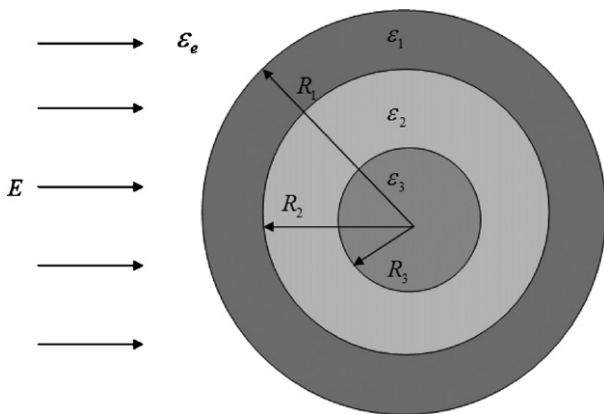


Fig. 3. A schematic description of the three-phase composite sphere model by Friedman [179].

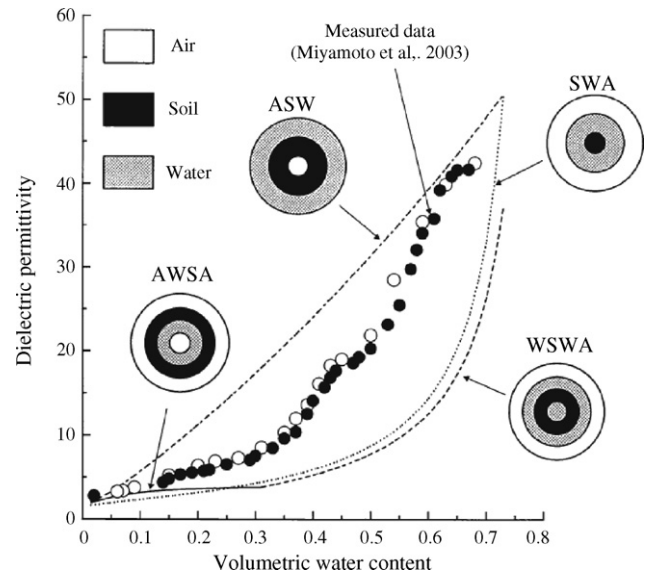


Fig. 4. Predictions by the composite sphere models compared with the experimental data [169]. ASW refers to air–solid–water arrangement; SWA, solid–water–air; AWSA, air–water–solid–water; WSWA, water–solid–water–air. The four-layer model uses AWSA arrangement when the volumetric water content is less than 0.31 and WSWA otherwise.

Miyamoto et al. [182] expanded Friedman's three-layer composite sphere model into four layers. Fig. 4 shows the predicted results using the three- and four-layer composite sphere models, respectively, in comparison with the experimental data. The results indicate that no single model can give reasonable predictions for the three-phase materials. Consequently, linear and nonlinear [179] weight functions were proposed to combine two or more such arrangements, but no clues given on how these weight functions were determined.

In a separate effort, Gori and Corasaniti [183] built up a cubic cell model for thermal conductivity of three-phase porous media. Water absorbed was considered to either cover the solid particles or form liquid-bridges between different particles. Analytical models were thus derived. Unfortunately, the critical water content for liquid-bridge formation was unknown and had to be determined empirically, hence causing gross errors in predictions.

2.2. Limitations and challenges

Although theoretical models for predictions of effective properties of complex materials have been extensively explored, the inherent limitations in these models greatly restraint their capability. The limitations in the existing theoretical models, and thus the challenges in developing new ones, are summarized below.

- (i) Most existing theoretical models are based on simplified physics with certain over-idealized assumptions. This may make the models easy and quick to use, but the simplifications also restrict the models to only simple structures.
- (ii) Any efforts in combining the models for more complex structures will lead to escalating in model complexity and computational costs. Most modifications to improve the accuracy of the models will in turn narrow their applicability.
- (iii) The empirical parameters introduce factors with no physical significance, whose values have to be determined case by case, thus rendering the models more difficult to use.
- (iv) Most existing theoretical models can only handle simple structures and thus become powerless once encountering complex materials. Consequently, none of the existing models

is able to tackle directly the effects of morphological changes in the microstructure on the material properties.

- (v) The existing theoretical models are largely incapable of dealing with the issue of phase interactions in multiphase systems, such as in a liquid–solid wetting process, the liquid phase distribution and their collective influence on the overall effective properties of the materials.
- (vi) Even for the relatively successful theoretical models, they can only calculate the properties of existing materials, rather than make predictions for new material. Therefore, they are not of much value in optimizations or design for novel materials.

3. Numerical methods

Given the limited power of the existing theoretical models in dealing with complex materials, the numerical methods are becoming increasingly important and more widely used in material science and engineering [184,185]. Especially, the rapid development of computational techniques in the past decades has tremendously enhanced our numerical capacities in modeling the multiphysical behaviors of multiphase materials, and enabled more accurate and robust approaches in prediction and design of more novel material systems. As stated repeatedly before, the effective properties of a complex material are determined by the collective contributions of the individual components, and by their internal structures. As a result, a complete numerical determination of the effective properties of multiphase media has to include such two major steps as first to reproduce properly the multiphase microstructures using computer algorithms, and then to solve the relevant transport governing equations (partial differential equations) with acceptable efficiency and accuracy.

3.1. Structure characterization and reproduction algorithms

3.1.1. Structure characters of multiphase complex materials

Considering the random and irregular microstructures of multiphase materials, at least five major structural characteristics can be identified:

Heterogeneity: Multiphase complex materials are made of two or more components/phases which are rarely distributed uniformly, and each component has its own properties and proportion, and thus contributes towards the effective system properties differently [186,187].

Interactions: As a result of mixture, both the phase distributions and inter-phase interactions become highly essential for the overall material behaviors [13,14].

Structure Geometrical Varieties: The microstructures of the complex media can be roughly divided into three distinct types: particle-like, fiber-like and netlike. As the property and geometry, distributions, inter-connections and couplings are totally different between each type, no generalized algorithms have been established to tackle such variations.

Randomness: Microstructures of multiphase materials mostly have strong stochastic characteristics, i.e., the shape, location and orientation of the structure elements, and the connections between them are all random to certain degree. For this reason, there are nearly no two materials, or even no two pieces of the same material, that possess exactly the same microstructure in every detail. The concept of the *equivalent* structures becomes more meaningful, i.e., structures formed based on certain statistical information from the original material and yielded the same effective properties. Such statistical information from real microstructures makes an equivalent structure realizable using computer algorithms [188].

Multiscale Hierarchy: As the rapid development of the microscopy technique, more observations and measurements have indicated that the microstructures of porous materials are actually of hierarchical multiscale, meaning each single “element” at one scale level can show a porous microstructure of its own at a still lower level [189,190]. The multiscale microstructure and its effects on material properties are a very interesting and important topic for material design.

3.1.2. Material structure reproduced in a computer

Several methods have been proposed to reconstruct the microstructures of multiphase materials using computers, and they can be divided into two classes/levels based on the methodologies. The methods at the primary level are the so-called apparent-similarity methods. The Random Location of Obstacles is the simplest one for two-phase granular microstructures. Each imaginary obstacle stands for a particle when the particle geometry details are negligible [191,192]. For instance, Tacher et al. [193] presented a discrete reduced-distance method to generate spherical/elliptical two-phase granular porous media. Based on Tacher's work, Pilotti [194] developed a grain sedimentation algorithm. Yang et al. [195] and Li et al. [196] used the assemblies of three-dimensional spheres with random size to reconstruct the microstructures of porous media. All these methods indeed created two-phase structures with random size and details. However, none of them can deal well with the interactions between the grains, thus unsuitable for energy/electric transfer problems that are extremely sensitive to contacts.

Given the significant influences of the geometric details such as the element shapes, orientations and connections, on the materials properties, a few newer methods aimed at approaching the real structures in more geometric details have been proposed, the so-called detail-similar methods. As the microscopy instruments and the observation technologies are well developed now, the image mapping has become a highly powerful tool for this purpose [197,198]. Better reconstruction processes have been used to generate two-phase [199,200] and multi-component [201,202] random structures of porous materials based on the digital microtomographic information and statistical correlation functions. A similar algorithm has been found in the soil research, termed as the Markov chain Monte Carlo method, which created two-dimensional structures with satisfactory agreement using the scanned images of real soil samples [203,204]. More about these reconstruction methods based on image mapping can be found in some review papers [187,202,205] and books [206,207]. For fibrous porous materials, Pan et al. have done a series of analysis to theoretically characterize the microstructure using the statistical density distribution function approaches [26,208].

Moreover, for multiphase materials, their microstructures can be influenced by the phase interactions. When such interactions are non-negligible, approaches have to be developed to reflect the influences during structure generation. To our best knowledge, this issue has seldom been systematically investigated. Losic et al. [201] proposed a reconstruction process with given phase probabilities and an overall correlation function to form lamellar clay films on solid surfaces and dispersed clay dots on solid structures. A few other researchers used the liquid-bridge structures for water distribution in unsaturated porous media [54,209,210]. This model may be valid for very smooth, hydrophobic and well contacted solid spheres, yet cannot be generalized for random porous media. In addition, Mohanty [211] adopted a Monte Carlo annealing algorithm to generate unsaturated porous media by using the law of lowest interfacial energy, but it failed to differentiate various liquid–solid interactions.

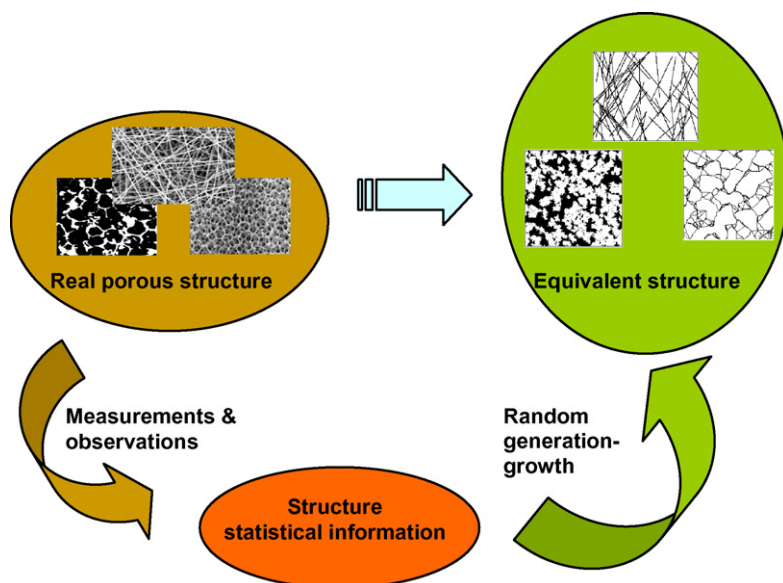


Fig. 5. Microstructure reproduction schematic of the random generation-growth method.

3.1.3. A random generation-growth method

The stochastic and statistical characteristics are two key natures in the microstructures of complex multiphase materials, as discussed above. Such stochastic characteristics reveal two things: (i) even in the real world, it is hard to find two materials that have exactly the same microstructure in every detail. This indicates that it is not necessary to duplicate in computer algorithm the microstructure of real materials in the exact duplicate. (ii) Random factors have to be incorporated into the reproduction process. The statistic characteristics also indicate two clues: (i) we can reproduce an equivalent microstructure for each real structure, where only the effective factors contributing to the material properties are taken into account; (ii) the equivalent microstructure owns the same major geometric statistical features as the real one but not in every detail. Based on these characteristics and inspired by the cluster growth theory [212], Wang et al. [17,213–216] proposed a multi-parameter random generation-growth method to reproduce the random multiphase microstructures using given statistical information. The basic idea of the method is shown in Fig. 5. The random generation-growth (RGG) method is designed to reproduce structural assemblies of elements with random sizes, locations and orientations, and connections, each of which grows from also randomly distributed seeds and the growth is guided by a few given probabilistic growth rates. For different types of microstructures (granular, fibrous or netlike), the algorithms will be different but still bear the same principles.

3.1.3.1. Granular structure. The random generation-growth algorithm for granular media, also termed as the Quartet Structure Generation Set (QSGS) [17,213] in which four parameters are identified for controlling the internal porous structure, can be described as follows.

Before initiation, one has to determine among the different phases in a system a non-growing phase and the rests are the growing ones. For generality, we call the growing phase as the n th phase, where $n = 2$ to N , the total number of phases in the system. Customarily and without losing generality, the discrete phases are normally taken as the growing phases. For example, rocks and moisture are the growing phases in unsaturated sands, whereas gas is the growing phase in polyurethane foams. Then the growing process follows the steps below.

(I) Randomly locate the cores of the first growing phase in a grid system based on a core distribution probability, c_d , whose value is no greater than the volume fraction of the phase. Each cell in the grid will be assigned a random number by a uniform distribution function within $(0, 1)$. Each cell whose random number is no greater than c_d will be chosen as a core; (II) Expand every element of the growing phase to its neighboring cells in all directions based on each given directional growth probability, D_i , where i represents the direction. Again for each growing element, new random numbers will be assigned to its neighboring cells. The neighboring cell in direction i will become part of the growing phase if its random number is no greater than D_i ; (III) Repeat the growing process of (II) until the volume fraction of the first growing phase reaches its given value ϕ^2 (if the growing phase is gas, ϕ^2 is more often expressed as the porosity ε); (IV) As to the next growing phase, there are two cases to consider depending on its interaction with the existing phase(s). If this phase is an equivalent discrete phase as the existing growing phase, such as multi-component mixture, it grows from separate seeds, which is very similar as the first growing phase described in (I)–(III). Otherwise, we have to consider the constraint by and interaction with the existing phase(s). For such cases, the n th phase ($n > 2$) will grow based on a phase interaction growth probability, $I_i^{n,m}$, which represents the growth probability of the n th phase on the m th phase along the i th direction; (V) Stop the n th phase growth once its volume fraction reaches the given value ϕ^n ; (VI) Repeat the next phase growth as described in (IV) and (V) until $n = N$; (VII) The spaces not occupied at the end represent the non-growing phase.

Thus, the four parameters (c_d , D_i , ϕ^n , and $I_i^{n,m}$), essentially control the microstructural characteristics of the generated porous media based on our QSGS process. The parameters can be determined through the statistical analysis of measured data, such as from the X-ray microtomography technique, or through first principle modeling such as molecular dynamics (MD) simulations. Each parameter has physical significance, rather than just an empirical factor.

The core distribution probability c_d is defined as the probability of a cell to become a core of the first growing phase on which growth or expansion of the first phase originates. The value of c_d indicates the number density of growing cores for the first growing phase, to reflect the statistical distribution of the first growing

phase throughout the system. For a given porosity, the average volume of each solid particle V_s could be related with c_d as: $V_s = (1 - \varepsilon)V/(N_c \cdot c_d)$ where V represents the total volume of system, and N_c the total cell number. The c_d value thus also controls the degree of structure details of a system; a smaller c_d leads to a finer description of the microstructures including particle/pore shapes and inter-particle/pore connections, etc. However, a small c_d value will also decrease the statistical particle numbers for a given grid size and thus increase the computation fluctuation.

The directional growth probability D_i is defined as the probability for a yet-to-be-occupied cell to merge into a neighboring cell in the i th direction to become part of the growing phase. An appropriate arrangement of the directional growth probabilities may lead to an isotropic structure. In other words, the growth probabilities can be adjusted to control the degree of anisotropy. For two-dimensional cases specially, each square cell has eight growing directions to its neighbors, as seen in Fig. 6. There are four main directions (1, 2, 3, 4) and four diagonal directions (5, 6, 7, 8). To obtain an isotropic structure in such systems, we set both the main directional growth probabilities D_{1-4} and the diagonal directional growth probabilities D_{5-8} into respective constants in each group, and set both constants in a fixed ratio. For instance, by designating the probabilities ratio, $D_{1-4}:D_{5-8} = 4$, we get the directional growth probability consistent with the equilibrium density distribution function for isotropic materials [217]. For three-dimensional structures, a similar probabilities ratio was used [218], yet more validations are needed in the future work. The relative value instead of the absolute value of D_i actually controls the anisotropy of structure.

For multiphase porous media systems ($n \geq 3$), the interactions between different discrete phases become even more complex, and we have to consider the effects of such interactions during the phase growth. Such effects are important especially for instance in unsaturated porous media soaked by a liquid that wets other phases in the system differentially. In such systems, the growth order of the various phases is important. Generally the solid phase is selected as the first growing phase and then the liquid phase grows under the influences of phase interactions. The phase interaction growth probability, $I_i^{n,m}$, i.e., the growth probability of n th phase on the surface of m th phase along the i th direction, is hence introduced to account for this influence by assigning different values to $I_i^{n,m}$ for different materials. The value of the phase interaction growth probability $I_i^{n,m}$ could be determined by analyzing the scanned pictures of phase distributions or by calculating from the wetting properties directly.

Fig. 7 shows six schematic illustrations of the porous structures generated using the QSGS method, where the stochastic characteristics are depicted very realistically in the figures. The first four figures represent two-phase cases, where the white area corresponds to the growing phase (solid) and the black the non-growing phase (gas). The parameters for Fig. 7a are $c_d = 0.01$, $\phi^s = 0.3$, $D_{1,3} = D_{2,4} = 4D_{5-8}$. Fig. 7b shows the case with a larger solid volume fraction ϕ^s , i.e., both the volume and the inter-particle connections of the solid phase increased. Comparison between Fig. 7b and c shows the effect of the core distribution probability c_d on the generated microstructure, and a higher value of c_d leads to a more uniform phase distribution of the medium. When the directional growth probability is not the same in every direction, the isotropy will be destroyed. Fig. 7d shows the generated anisotropic structure, where the horizontal growth probability is ten times of the vertical one, $D_{1,3} = 10D_{2,4}$ and $D_{2,4} = 4D_{5-8}$. Fig. 7e and f show the phase distributions of three-phase porous medium using different phase interaction probabilities. The black is the non-growing phase (gas), the grey is the first growing phase (solid), and the white is the second growing phase (liquid). The phase interaction probability dictates

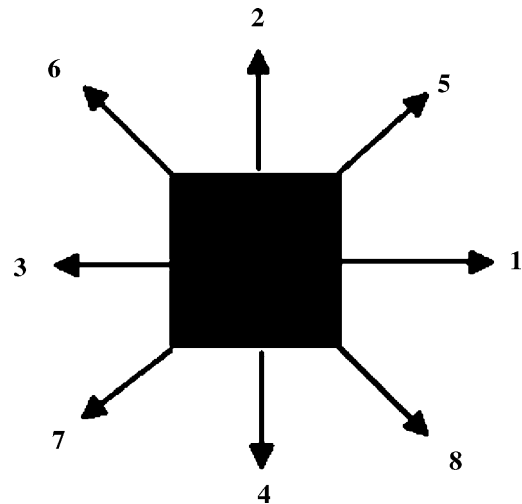


Fig. 6. Eight growth directions of each cell for 2D granular systems.

the distribution status of the second growing phase. A high value of liquid–solid interaction means a strong wetting property of the liquid on the solid surface so that the liquid will distribute like a film on the solid surface, as shown in Fig. 7e. On the contrary, a strong liquid–liquid interaction probability leads to a high degree of liquid aggregation, and the liquid exists as droplets or liquid-bridges on the solid particles (see Fig. 7a–f).

Compared with most of the previous reconstruction methods, the QSGS method has the following merits: (i) Both stochastic and statistic features are incorporated into the generation-growth process, and therefore the generated microstructure is closer to a real one. (ii) Each of the parameters in the algorithm has a distinct physical meaning, instead of just being an empirical coefficient. (iii) The multi-body connection problem is thus solved. (iv) The method is efficient without turning to any iteration process. (v) The algorithm can be extended straightforwardly to three-dimensional and/or multiphase cases, and is suitable for parallel computing.

3.1.3.2. Fibrous structure. The random generation-growth algorithm for fibrous structures is much easier if one assumes that each fiber is represented by a straight line with given diameter d and length l , and located by its core position and orientation angle θ , as illustrated in Fig. 8. Similar assumptions can be found in many previous studies [219]. The generation process for two-dimensional (2D) structures is conducted as follows [214].

(I) Randomly locate the fiber cores based on a core distribution probability, c_d , and the core position distribution function, F . The core distribution probability c_d is defined as the probability of a point to become a core of the fiber, and this c_d value is related to the fiber number density. The core position distribution function F could be a uniform, a normal or any other distribution function of position (x, y) ; (II) randomly assign an orientation angle θ to each fiber core, and θ ranges within $[-\theta_{lim}, \theta_{lim}]$; (III) grow fibers from each core along both directions of the orientation θ for fiber length and crosswise for fiber thickness; (IV) stop growth once fiber dimensions, d and l , reach the specified values, or the overall porosity attains the given level ε . Thus, there are six parameters, c_d , F , θ_{lim} , d , l , and ε collectively controlling the resulting structure.

Fig. 9 shows an example of a generated fibrous structure in 200×200 grids for $c_d = 0.0025$, $d = \delta_x$, $l = 100\delta_x$, $\theta_{lim} = \pi/2$, and a uniform distribution. The fibers are in dark and the continuous phase in white. This 2D algorithm has been extended to 3D by simply adding another orientation angle to control the fiber growth direction in the 3D space [215].

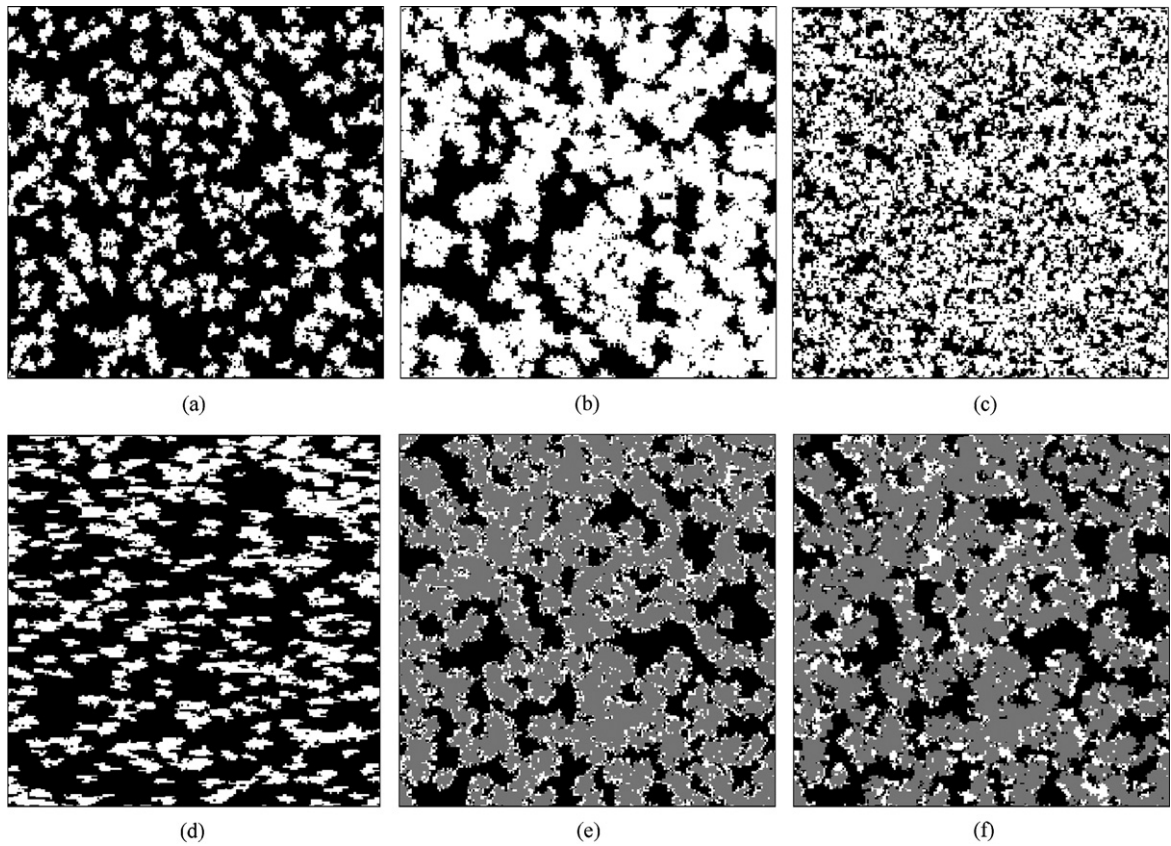


Fig. 7. Schematics of the generated porous structures using QSGS method in 200×200 grids. (a) $c_d = 0.01$, $\phi^s = 0.3$; (b) $c_d = 0.01$, $\phi^s = 0.6$; (c) $c_d = 0.1$, $\phi^s = 0.6$; (d) $c_d = 0.01$, $\phi^s = 0.3$, $D_{1,3}:D_{2,4} = 10$; (e) $l_1^l:l_1^s = 1$; (f) $l_1^l:l_1^s = 10$.

3.1.3.3. Netlike structure. The netlike structures, such as the open-cell foam, are a little more complex, and few approaches available in the public can tackle such structures with an acceptable accuracy. Calmidi and Mahajan [22] and Bhattacharya et al. [20] depicted this type of structure using an array of hexagonal cells with lump formed at the intersection. Boomsma and Poulikakos [220] modeled such structures in three dimensions in the form of tetrakaidecahedral cells with cubic nodes at the intersection.

However, such existing models have to use an empirical parameter to account for the effects of the inter-cell connections.

Under the same idea of random generation-growth method, the main process of reconstruction for netlike structures for a two-dimensional two-phase (2d2p) case can be described as follows.

- (I) Stochastically distribute the cores as the net nodes on a lattice system based on a give probability c_d , similar to the other generation processes;
- (II) For each net node, search outward to the

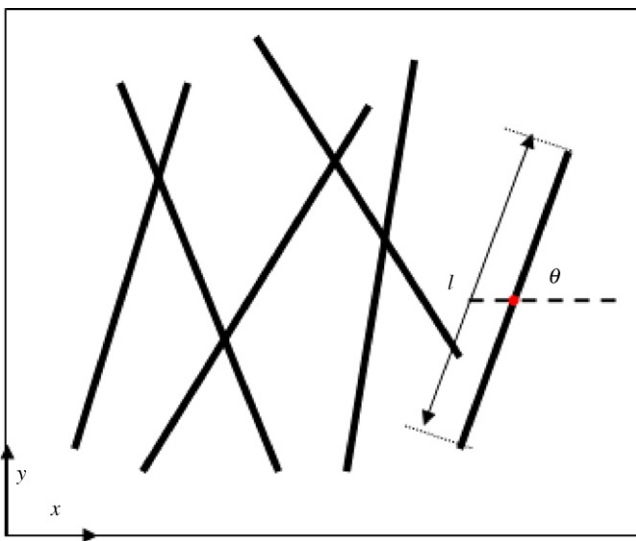


Fig. 8. Growing fibers and parameters.

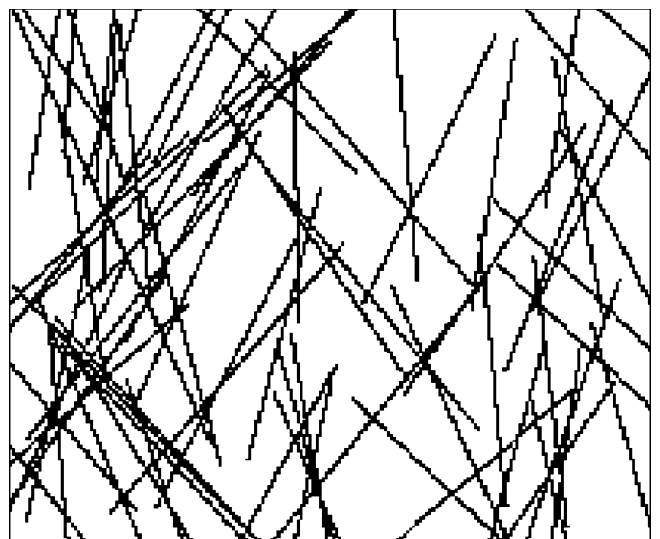


Fig. 9. A reconstructed fibrous structure.

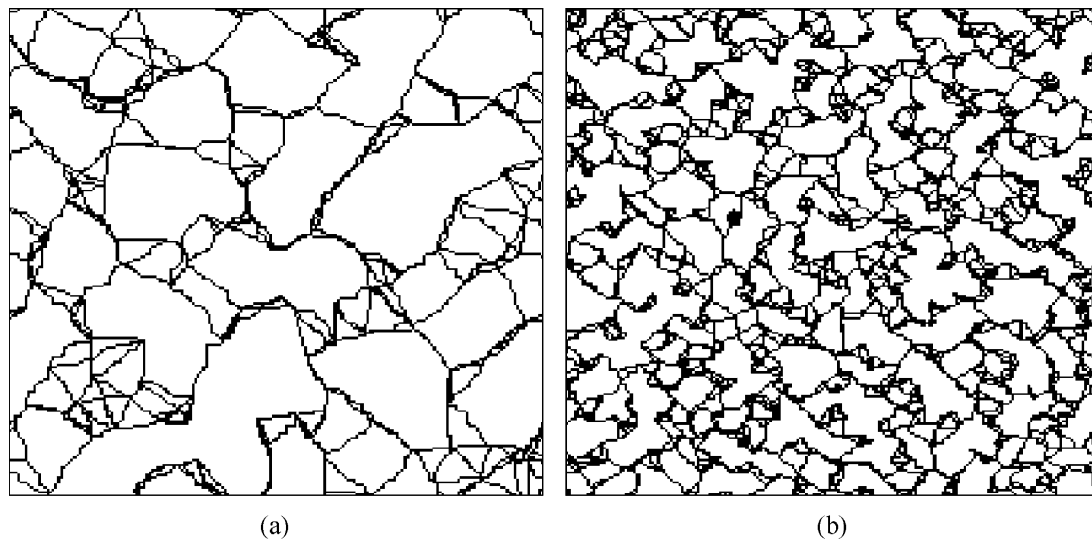


Fig. 10. A reproduced netlike random microstructure of a two-phase system. The dark is the solid and the white the air. (a) $\varepsilon = 0.8888$ and (b) $\varepsilon = 0.7373$.

neighboring nodes and randomly select N_n of them as the link nodes; here N is determined based on the features of specific porous media. Genetic algorithm or other searching algorithms could be used for this process. (III) Grow link lines from a net node to each of its N link nodes. Again the random rejection–acceptance rule is applied to the process and in the end every node will connect with other nodes with N_n link lines so as to form such a network. Fig. 10 shows two reproduced netlike structures on a 200×200 grid with $N_n = 4$.

3.2. Solutions of the governing laws

After the microstructures are reconstructed, the governing equations for transport in the materials need to be solved numerically for the effective properties of multiphase material systems. The conventional partial differential equation (PDE) solvers, such as finite difference method (FDM), finite element method (FEM) and boundary element method (BEM), have been applied to tackle the governing equations in multiphase media of heat transfer [221–227] and electric field transports [228–237]. However, the structural complexities bring in two difficulties. The first is the requirement of *grid refinements* for complex structures: the accuracy of such conventional numerical methods is strongly dependent on the grid size, so that an extra-fine grid is needed whenever the transport process is complex in physics and/or in geometry. Consequently, when dealing with multiphase transport problems in porous media with complex geometries, the extreme complexities and the corresponding computation intensity will in practice confine the computational domain in a very limited area. The second is the *conjugate constraints* at interfaces between different phases: for steady electric field transport through multiphase structures for instance, electric potential and flux continuities have to be ensured at the interfaces when solving the governing equations, thus demanding enormously high computational resources for a porous medium with innumerable interfaces in the structure.

Recently the stochastic methods for representing the perturbations in porous media have gained much attention [238,239]. Shoshany et al. [240] and Barta and Dieska [241] modeled the thermal conductivity of porous materials using the Monte Carlo method to reflect the structural fluctuations during the process. Yue et al. [242,243] developed a lattice gas automata method to predict the electric transport properties in two-dimensional

multiphase porous media. Owing to its easy implementation of multiple inter-particle interactions and complex geometry boundary conditions [218,244–250], and that in general the conservation laws can hold automatically without additional computational efforts [251–254], the lattice Boltzmann method (LBM) has recently been developed successfully for modeling of hydrodynamics [185,250,251], thermodynamics [255–257] and electrodynamics [254,258] in multiphase systems and the effective properties can be consequently calculated.

3.2.1. Governing equations

Let us consider thermal or electric transport through a multiphase material system as shown in Fig. 11. To determine the effective conductivities, a set of transport governing equations need to be solved. Considering a steady and pure thermal or electric transport process without contact resistance, radiation, phase change or other influences from the source, the governing equations can be summarized as follows.

Once the effective medium theory (EMT) is applicable [259], the thermal or electric transports in a multiphase medium is governed by a Laplace equation [231,236]:

$$\nabla \cdot (\lambda_n \nabla \Phi) = 0 \quad (15)$$

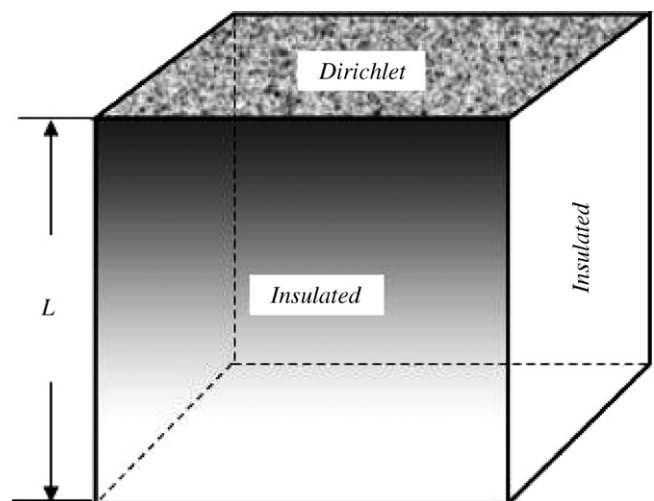


Fig. 11. Schematic diagram of domain and boundaries.

where λ_n is the local conductivity of the n th phase, which could be thermal conductivity or electric conductivity/dielectric permittivity for a given case, and correspondingly, Φ would be the thermal potential/temperature [221–227,260] or the electric potential [228–236,261].

Two points in Eq. (15) should be noted. First, only steady-state transport is described by the equation, because the unsteady terms have no contribution to the effective properties. Second, the local property (λ_n) should not be moved outside of the divergence operator since it changes its value with the position, leading to incorrect predictions [262].

At the interfaces between two phases (i and j) in equilibrium, the continuities of both potential and flux have to be satisfied, i.e.,

$$\Phi_{\text{int},i} = \Phi_{\text{int},j} \quad (16)$$

$$\lambda_i \nabla \Phi|_{\text{int},i} = \lambda_j \nabla \Phi|_{\text{int},j} \quad (17)$$

where the subscript “int” corresponds to the interfaces between phase “ i ” and “ j ”. Eq. (15) thus governs the distribution of potential Φ in the multiphase material, subject to the interface constraints in Eqs. (16) and (17). After the potential field is derived, the effective conductivity can be determined as

$$\lambda_{\text{eff}} = \frac{qL}{\Delta\Phi} \quad (18)$$

where q is the steady flux through the material between the potential difference ($\Delta\Phi$) over a thickness L .

Very similar governing equations have been derived for mechanical elastic properties with the assumptions of steady small elastic strain in the direction of the force with negligible multi-dimensional deformation effects [263–265]. For the mechanics equation, λ_n in Eq. (15) represents the local mechanical modulus, either Young’s modulus or shear modulus, Φ the displacement in the direction of force, and q the stress in a given direction. Unlike the other transport properties, such a governing equation for mechanical moduli has rarely been employed to numerical calculation of the effective properties of multiphase materials. The likely first attempt has shown successful applications [265].

3.2.2. A Lattice Boltzmann solver

The lattice Boltzmann method (LBM) is intrinsically a *mesoscopic* computational fluid dynamics (CFD) approach based on the evolution of statistical distribution on lattices, and has achieved considerable success in simulating fluid flows and associated transport phenomena [251,253]. For more details about the LBM, one can consult excellent book [252] and review papers [185,251]. The most important advantages of LBM include the easy implementation of both multiple inter-particle interactions and complex geometry boundary conditions [218,244–250]. Conservations can generally hold automatically without additional computational efforts [252,254,256,266].

The original lattice Boltzmann model for single time Bhatnager–Gross–Krook (BGK) relaxation collision operator [251] is used to solve the Navier–Stokes (NS) equation for fluid flow. The evolution equation is

$$f_\alpha(\mathbf{r} + \mathbf{e}_\alpha \delta_t, t + \delta_t) - f_\alpha(\mathbf{r}, t) = -\frac{1}{\tau_v} [f_\alpha(\mathbf{r}, t) - f_\alpha^{\text{eq}}(\mathbf{r}, t)] \quad (19)$$

with a local equilibrium distribution function

$$f_\alpha^{\text{eq}} = \omega_\alpha \rho_f \left[1 + 3 \frac{\mathbf{e}_\alpha \cdot \mathbf{u}}{c^2} + 9 \frac{(\mathbf{e}_\alpha \cdot \mathbf{u})^2}{2c^4} - \frac{3\mathbf{u}^2}{2c^2} \right] \quad (20)$$

and

$$\tau_v = 3\nu \frac{\delta_t}{\delta_x^2} + 0.5 \quad (21)$$

where τ_v is the viscosity-based dimensionless relaxation time, ν the kinematic viscosity, δ_x the lattice constant, and δ_t the time step.

It has been proved that through the Chapman–Enskog multi-scale expansion, the Lattice BGK equation is consistent with the incompressible Navier–Stokes equation [251,267]:

$$\frac{\partial \mathbf{u}}{\partial t} + \mathbf{u} \cdot \nabla \mathbf{u} = -\nabla p_f + \nabla \cdot (\nu_f \nabla \mathbf{u}) \quad (22)$$

Inspired by this process, and by treating the generalized governing equation (Eq. (15)) as a special case of the NS equation (Eq. (22)), the lattice evolution equation can be expressed as [256,257]:

$$g_\alpha(\mathbf{r} + \mathbf{e}_\alpha \delta_t, t + \delta_t) - g_\alpha(\mathbf{r}, t) = -\frac{1}{\tau_n} [g_\alpha(\mathbf{r}, t) - g_\alpha^{\text{eq}}(\mathbf{r}, t)] \quad (23)$$

where g_α^{eq} is the local equilibrium distribution in each direction, \mathbf{e}_α the discrete lattice velocity, and τ_n the dimensionless relaxation time for local phase. The equilibrium distribution of the evolution variable, g_α , for the two-dimensional nine-speed (D2Q9) model is

$$g_\alpha^{\text{eq}} = \begin{cases} 0, & \alpha = 0 \\ \frac{\Phi}{6}, & \alpha = 1, 2, 3, 4, \\ \frac{\Phi}{12}, & \alpha = 5, 6, 7, 8 \end{cases} \quad (24)$$

the microscopic velocity

$$\mathbf{e}_\alpha = \begin{cases} (0, 0), & \alpha = 0 \\ (\cos \theta_\alpha, \sin \theta_\alpha), & \theta_\alpha = (\alpha - 1)\pi/2, \quad \alpha = 1, 2, 3, 4, \\ \sqrt{2}(\cos \theta_\alpha, \sin \theta_\alpha), & \theta_\alpha = (\alpha - 5)\pi/2 + \pi/4, \quad \alpha = 5, 6, 7, 8 \end{cases} \quad (25)$$

and the dimensionless relaxation time

$$\tau_n = \frac{3}{2} \frac{\lambda_n}{c^2 \delta_t} + 0.5, \quad (26)$$

where δ_t is the time step, and c is the lattice speed whose value in theory can take any positive value provided the resulting τ_n value is within (0.5, 2) [254,256].

For a three-dimensional fifteen-speed (D3Q15) model shown in Fig. 12, there are

$$g_\alpha^{\text{eq}} = \begin{cases} 0, & \alpha = 0 \\ \frac{\Phi}{9}, & \alpha = 1-6, \\ \frac{\Phi}{24}, & \alpha = 7-14 \end{cases} \quad (27)$$

$$\mathbf{e}_\alpha = \begin{cases} (0, 0, 0), & \alpha = 0 \\ (\pm 1, 0, 0)c, (0, \pm 1, 0)c, (0, 0, \pm 1)c, & \alpha = 1-6, \\ (\pm 1, \pm 1, \pm 1)c, & \alpha = 7-14 \end{cases} \quad (28)$$

and

$$\tau_n = \frac{9}{5} \frac{\lambda_n}{c^2 \delta_t} + 0.5, \quad (29)$$

Both the potential and flux can then be calculated according to [268]

$$\Phi = \sum_\alpha g_\alpha, \quad (30)$$

$$q = \left(\sum_\alpha \mathbf{e}_\alpha g_\alpha \right) \frac{\tau_n - 0.5}{\tau_n}. \quad (31)$$

Once the potential field is solved, the effective conductivity, λ_{eff} , can be determined as

$$\lambda_e = \frac{L \cdot \int q \cdot d\mathbf{A}}{\Delta\Phi \int d\mathbf{A}}, \quad (32)$$

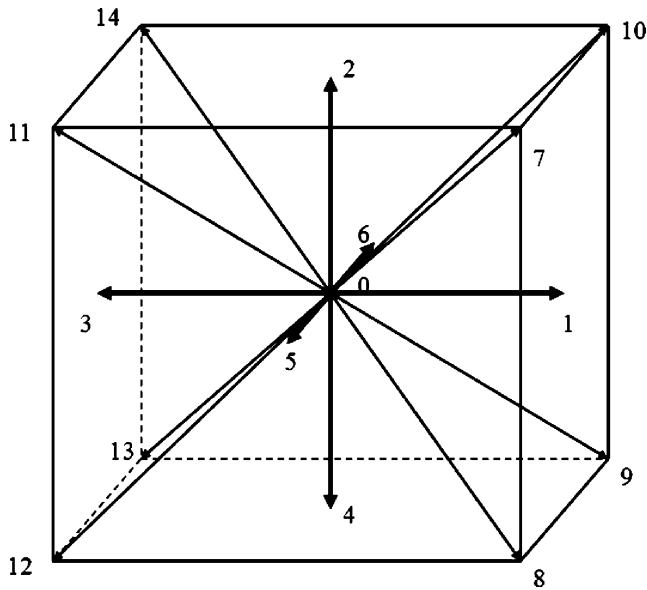


Fig. 12. The lattice direction system (α) for D3Q15 model.

For the Dirichlet boundary treatment, we follow the bounce-back rule of non-equilibrium distribution proposed by Zou and He [269]:

$$g_\alpha - g_\alpha^{eq} = -(g_\beta - g_\beta^{eq}), \quad (33)$$

where α and β represent the opposite directions, and the equilibrium distribution can be calculated based on the local boundary temperature. For the insulated boundaries, a specular reflection treatment is implemented to prevent heat flux from leaking along the insulate surfaces. It has been proved that the current boundary treatments have second-order accuracies [269].

3.2.3. Benchmarks

The lattice Boltzmann algorithm and codes were numerically validated by two basic structures of dual-component systems: the Parallel mode and the Series mode. Assuming the conductivity of each component is k_1 and k_2 , respectively, the theoretical solutions predict the effective conductivities as $(k_1 + k_2)/2$ for the parallel mode and $1/(1/2k_1 + 1/2k_2)/2$ for the series mode [111,112]. Table 2 lists the calculated effective thermal conductivities by the present model in comparison with the theoretical solutions for different values of $k_1:k_2$. We keep k_1 as 1.0 while changing k_2 from 10 to 10,000. Such a large contrast between k_1 and k_2 leads to a longer computational time for any algorithms to converge, yet provides a more strict test on the LB model. The deviations in Table 2 between the predictions are no greater than 0.006% for the Parallel mode and 0.765% for the Series mode even under such large conductivity contrasts, showing a good accuracy of the lattice Boltzmann method.

Next, the lattice Boltzmann method was validated by simulating the transport process in functionally graded materials with

continuously varying properties. Consider the cube problem with given property gradations only along the z -axis, and is position dependent only. Let the potential at the top surface maintain at Φ_T and that at the bottom $\Phi_B = 0$. The conductivity at the bottom surface is λ_0 . Three cases are considered with, respectively, the quadratic, exponential and trigonometric property gradations in the z -direction.

Quadratic:

$$\lambda = \lambda_0(1 + \beta z)^2 \quad (34)$$

Exponential:

$$\lambda = \lambda_0 e^{2\beta z} \quad (35)$$

Trigonometric:

$$\lambda = \lambda_0(a_1 \cos \beta z + a_2 \sin \beta z)^2 \quad (36)$$

The corresponding steady analytical solutions of the potential distribution for these three cases are [226]

Quadratic:

$$\Phi = \frac{\sqrt{\lambda_0}(1 + \beta L)z\Phi_T}{\sqrt{\lambda}L} \quad (37)$$

Exponential:

$$\Phi = \Phi_T \frac{1 - e^{-2\beta z}}{1 - e^{-2\beta L}} \quad (38)$$

Trigonometric:

$$\Phi = \frac{\sqrt{\lambda_0}(a_1 \cos \beta L + a_2 \sin \beta L)\Phi_T \sin \beta z}{\sqrt{\lambda} \sin \beta L} \quad (39)$$

Fig. 13 compares the potential distributions of the three analytical solutions, with our numerical predictions using the present lattice Boltzmann method. The dimensionless parameters used are $\lambda_0 = 10$, $\beta = 2$, $\Phi_T = 1$, $L = 1$, and $a_1 = a_2 = 1$. The solid lines are the analytical solutions and the symbols are our numerical predictions. $200 \times 200 \times 200$ 3D grids are used in the simulations. The excellent agreements in the figure thus validate the present algorithm and the computation codes.

On the computational efficiency, the lattice Boltzmann method has been compared with the conventional CFD methods by simulating the same conjugate heat transfer problem in thick straight-wall channels [256]. Fig. 14 shows the calculated temperature at the middle of the channel varying with the mesh number in the x -direction, by the two different methods. The results indicated that the conventional CFD (performed by Fluent 6.22) needs at least 5–10 times finer grid divisions to reach the same accuracy as the LBM. Such an advantage of LBM will become much more apparent in dealing with complex geometry, a key feature of porous media.

Table 2
Comparisons between our predicted results and existing theoretical solutions, $k_1 = 1.0$

Results, $k_1:k_2$	Parallel mode			Series mode		
	Theoretical value	Present predictions	Relative deviations (%)	Theoretical value	Present predictions	Relative deviations (%)
1:10	5.500	5.500	0.000	1.818	1.815	0.165
1:100	50.50	50.50	0.000	1.980	1.976	0.202
1:500	250.5	250.5	0.000	1.996	1.991	0.250
1:1000	500.5	500.5	0.000	1.998	1.993	0.250
1:10,000	5000.5	5000.2	0.006	1.9998	2.0151	0.765

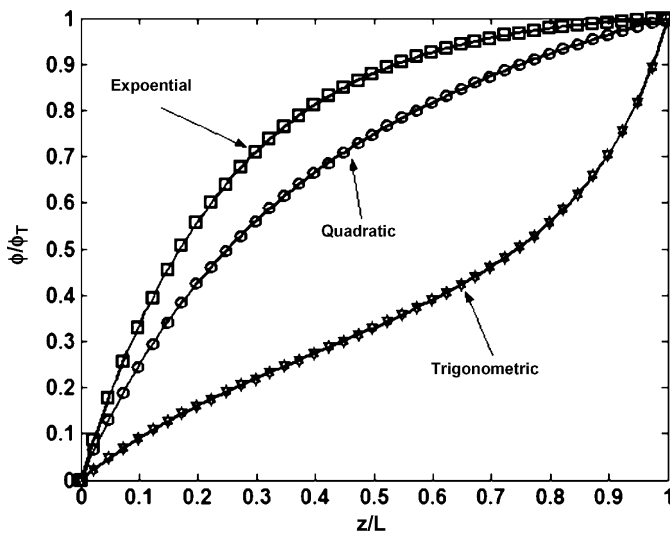


Fig. 13. Potential profiles in the z -direction. The parameters used are $\lambda_0 = 10$, $\beta = 2$, $\phi_T = 1$, $L = 1$, and $a_1 = a_2 = 1$. The solid lines are analytical solutions and the symbols are numerical predictions.

4. Applications

It is one of the most fundamental goals in materials science to establish connections between the macro behaviors of a material and the corresponding properties of each inclusion. Inherently, two major issues appeared—the internal morphology of the material formed by the constituents, and the interactions among themselves. However, even for simple cases, bringing these two factors into a theoretical treatment often poses as a challenge except for highly regular structures. Once materials become more complex with irregular internal morphology and formed by constituents of different phases, dealing with such issues turns into a daunting task.

However, in the set of novel mesoscopic numerical methods introduced in the last section, two steps were performed to tackle the issues. First, the equivalent multiphase microstructures were reproduced by a multi-parameter random generation-growth method based on the statistical information of real structures from experiments or existing data. Second, the related governing equations on transport processes were numerically solved by a high-efficiency lattice Boltzmann method. Such methods enable us

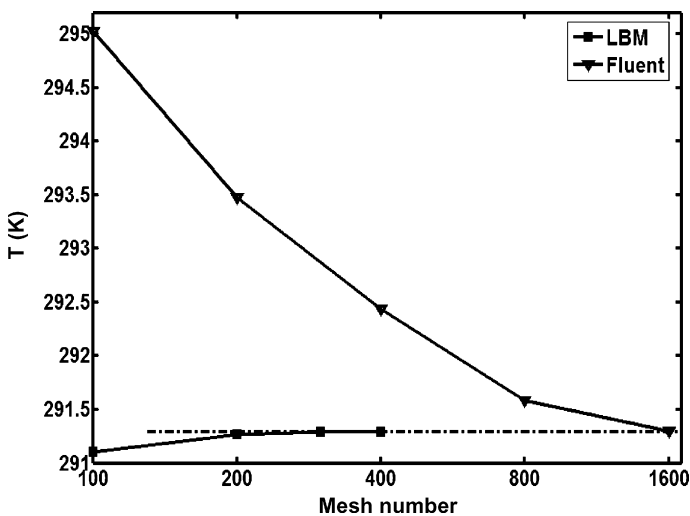


Fig. 14. Temperatures at the middle of the thick and straight-wall channel by CFD and LBM versus the mesh number in x -direction. Square grids are used.

not only to calculate the properties of the existing structures of materials, but also to predict those of new or even materials nonexistent in nature.

This section is to demonstrate the power of the new methods by dealing with several transport problems. For each problem, the methodology is first validated by comparing the yield predictions with the existing experimental data from the literature. Subsequently the major structure effects on the effective properties of these materials are systematically studied, including the morphology effects, anisotropy effects and size effects. For materials with three or more phases, the phase interaction effects on the effective properties are also treated. Finally as an extra application, the examination and comparison of available experimental techniques, based on the numerical results, are provided in Section 4.6.

4.1. Different physical properties in transport

As stated above, since some different physical processes share the same governing equations (Eqs. (15)–(17)) under certain assumptions, our new mesoscopic methods are employed below for predictions of various physical properties, including the thermal conductivity, the electric conductivity/dielectric permittivity, and the elastic moduli. The calculated results were compared with the existing experimental data.

4.1.1. Thermal conductivity

Among all physical properties of multiphase material systems, the thermal and electrical conductivities are the mostly studies ones due to their significance and wide applications. There are large number of experimental data available for validation purpose.

4.1.1.1. A two-phase granular composite. Consider a Cu/solder composite, where the Cu particles are uniformly dispersed in the solder mass [270]. To reproduce the two-dimensional microstructure of this two-phase granular composite using the QSGS [17], the solder is selected as the non-growing (first) phase and the Cu particles are the growing (second) phase. The structure is considered as isotropic. Since the Cu particle size was not provided in the literature [270] where the experimental data we collected, the parameter in QSGS on the growing phase size has to be estimated as $c_d = 0.01$. The component thermal conductivities are $k_{Cu} = 398.0$ W/m K, and $k_{solder} = 78.1$ W/m K [270]. Fig. 15

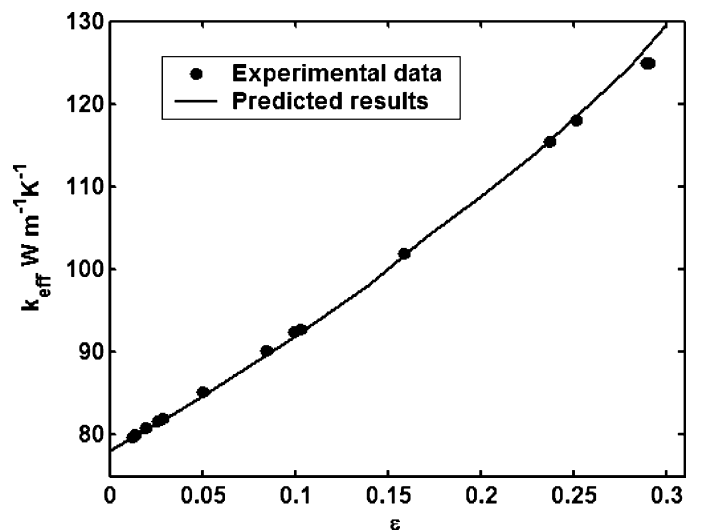


Fig. 15. Comparisons between predictions and experimental data for Cu/solder material. The experimental data is from Ref. [270]. The parameters are $k_{Cu} = 398.0$ W/m K and $k_{solder} = 78.1$ W/m K.

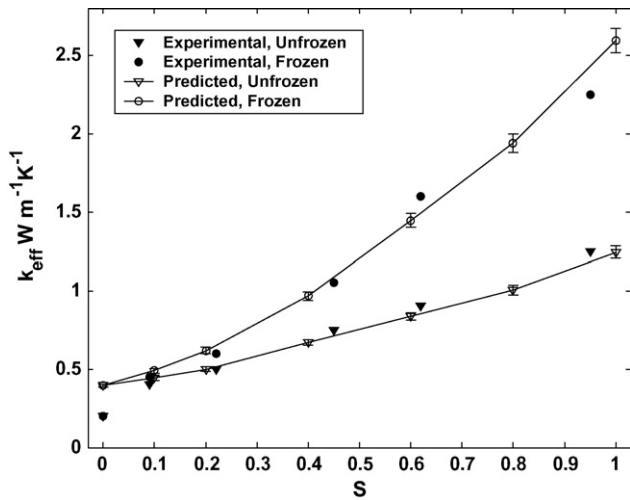


Fig. 16. Comparisons between predicted and experimental effective thermal conductivities of unsaturated porous sands in frozen and unfrozen states. The experimental data is from Ref. [271,273]. The parameters are $\varepsilon = 0.52$, $k_s = 2.85$ W/m K, $k_w = 0.5924$ W/m K, $k_g = 0.0249$ W/m K, and $k_{ice} = 2.38$ W/m K.

shows the effective thermal conductivities calculated by the new mesoscopic method, as a function of Cu volume fraction, ϕ_2 , compared with the experimental data from Ref. [270]. The numerical results agree with the experimental data fairly well.

4.1.1.2. *A three-phase granular material.* Unsaturated soil represents a typical case of three-phase granular material systems. Customarily, the porosity, ε , is defined as the total volume fraction of both air and the liquid. The degree of saturation, S , is the liquid volume fraction within the fluids. Therefore, the solid phase, the liquid phase and the gas phase have the volume fractions of $(1 - \varepsilon)$, εS and $\varepsilon(1 - S)$, respectively. To reconstruct a three-phase isotropic microstructure, the parameters used in QSGS are $c_d = 0.01$, and $I_i^{3,2} = I_i^{3,3}$ for each i -direction. Fig. 16 shows the predicted effective thermal conductivities versus the degree of saturation S at $\varepsilon = 0.52$ for moist porous brick sands, in both the frozen and unfrozen states. The thermal conductivities used in the simulations are $k_s = 2.85$ W/m K, $k_w = 0.5924$ W/m K, $k_g = 0.0249$ W/m K, and $k_{ice} = 2.38$ W/m K [271,272]. A 200×200 grid is used in the simulations, yielding the random fluctuation within 3%. The numerical results are compared with the experimental data [271,273]. Once again, good agreements are obtained with the experimental data for both frozen and unfrozen cases.

4.1.1.3. *Fibrous composites.* It has been attractive to use carbon fiber for its excellent performance acting as fillers in composite materials to improve the thermal, electrical and mechanical performances. One typical example is for nanofluids [31,274,275]. It has been reported that by just adding 1% volume fraction of carbon nanofibers into oil to form a nanofiber-in-oil suspension, the thermal conductivity of the oil was enhanced up to 150% [31]. However, the extremely high aspect ratio and the very small volume fraction of the nanofibers brought big challenges in reconstruction of such a fibrous structure. The predictions became fluctuated due to the low fiber loadings. In another case, Frusteri et al. [32,33] have recently measured the thermal conductivity of a phase change material containing carbon fibers. The fiber loading is much higher (up to 10 wt.%). Here we compare their experimental data with our mesoscopic numerical predictions. Because little structure information was provided with the experimental measurements, we have to estimate the statistical parameters for structure reproductions. To reduce the computational load, the

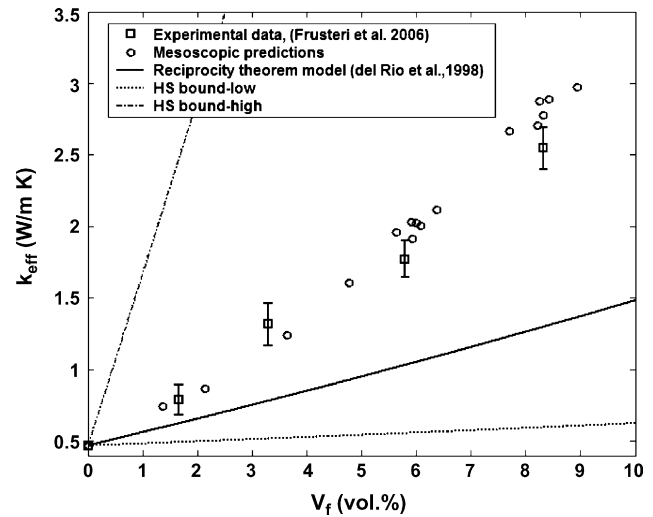


Fig. 17. Measured and predicted effective thermal conductivity of phase change materials containing carbon fibers. The properties used are $k_f = 180$ W/m K, $k_m = 0.47$ W/m K.

microstructure was reconstructed in a $60 \times 60 \times 60$ 3D grid system. To reflect the high-aspect ratio without losing the fiber-end transport effects, the fibers were generated with $L = 120$ by performing a periodic treatment when the growth met the boundaries. The width of each fiber was assumed as one unit grid size and the orientation angle of the fibers was uniformly random so that the structure was isotropic. The thermal properties used in our simulations are $k_f = 180$ W/m K and $k_m = 0.47$ W/m K [32]. Fig. 17 shows good agreement between our predictions and the measured data when the volume fraction is lower than 6%. When the fiber fraction is high, the inter-fiber contacts will affect the effective thermal property. Because no thermal contact resistance [276] is considered in our model, the predicted thermal conductivities are a little higher than, but still comparable with, the experimental data when the fiber fraction is high. The numerical relative errors due mainly to the fibers distribution randomness are at the same level as those of experimental measurements.

4.1.1.4. *Netlike structure.* Foam materials have shown good transport and mechanical performances at high porosities, because of the porous netlike microstructures. Their effective properties were severely underestimated when the traditional theoretical models were applied. Several new numerical approaches for regular structures have been proposed for such materials, but with some empirical parameters to account for the gap between the assumed regular structures and the actual materials [20,24,25,277]. The random generation-growth method has been used to reconstruct the netlike random microstructures of the foam materials on a $50 \times 50 \times 50$ grid [216], which could limit the fluctuations in the predictions to roughly smaller than 5%.

The predicted effective thermal conductivities of reticulated vitreous carbon (RVC) foams with water or air as the fluid media are compared with the existing experimental data [20] in Fig. 18. The component thermal conductivities used in the simulations are $k_{RVC} = 8.5$ W/m K, $k_{water} = 0.615$ W/m K and $k_{air} = 0.026$ W/m K [277,278]. The RVC-water predictions agree well with the experimental data while the RVC-air predictions are a little lower. We noticed that the ambient temperature was 25°C when performing the experimental measurements [20], therefore the underestimation of the effective thermal conductivity of RVC-air foams could result from the neglected thermal radiation. The effects of thermal

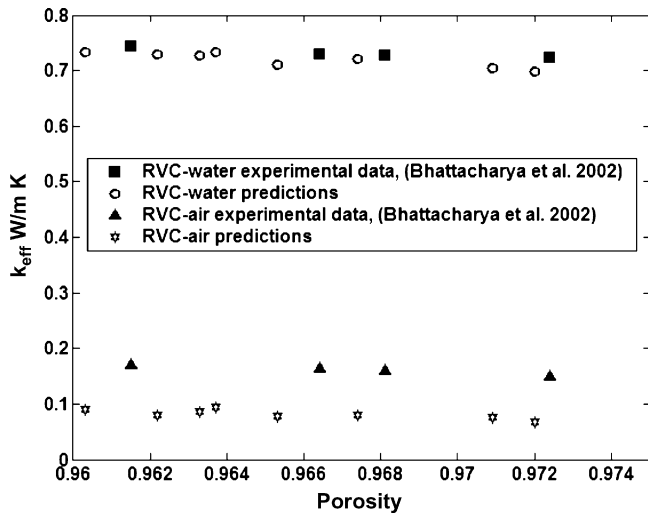


Fig. 18. Comparisons of effective thermal conductivities in RVC foams.

radiation may become more significant when the overall effective thermal conductivity of the media is relatively low.

To evaluate the contribution of the radiation heat transfer, Tao et al. [24] proposed a simple relationship to introduce the radiation effect into the thermal conductivity, k_{rd} , for the polyurethane (PU) foams as:

$$k_{rd} = \frac{16\sigma T^3}{3(42.038\rho_s V_s + 121.55)} \quad (40)$$

where σ is the Stefan–Boltzmann constant ($5.67 \times 10^{-8} \text{ W/m}^2 \text{ K}^4$), T the mean temperature, ρ_s the solid density and V_s the solid volume fraction.

Fig. 19 shows the predictions of effective thermal conductivities of PU foams at 286 K with and without the radiation modification, in comparison with experimental data [24,25]. The parameters used in the simulations are the thermal conductivity of PU solid $k_{PU} = 0.262 \text{ W/m K}$, the thermal conductivity of air at 286 K and under standard pressure $k_{air,sp} = 0.0252 \text{ W/m K}$, then at 286 K and under a lower pressure (nearly 2 Pa) $k_{air,lp} = 5 \times 10^{-7} \text{ W/m K}$,

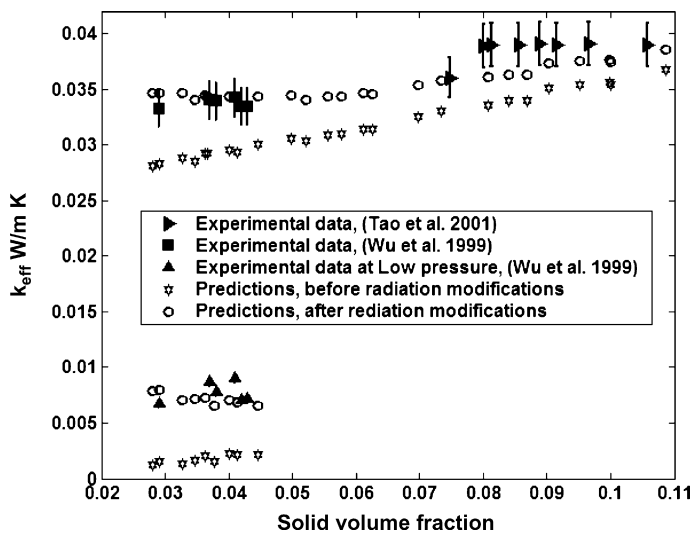


Fig. 19. Comparisons of effective thermal conductivities against the solid volume fraction in polyurethane foams. The solid symbols are experimental data, the stars are predicted results before radiation modifications and the circles are predictions after modifications.

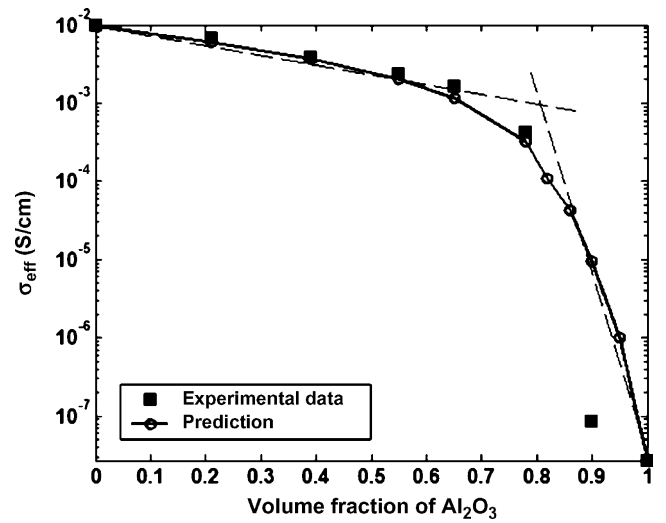


Fig. 20. Effective electric conductivities variation with volume fraction of Al_2O_3 for the granular $\text{Al}_2\text{O}_3/\text{Y-TZP}$ composites. The experimental data is from Ref. [42].

and the PU solid density $\rho_s \approx 800 \text{ kg/m}^3$ [278]. After the radiation modification the predicted effective thermal conductivities agree pretty well with the experimental data for PU foams under both standard air pressure and the lower air pressure as seen in Fig. 6. The results also show that the importance of radiation contribution decreases with an increasing solid volume fraction so that the two simulation results converge at high solid volume fraction, the radiation contribution accounting for almost 6% when the solid volume fraction is over 10% for 286 K at standard air pressure condition, as illustrated in Fig. 19.

4.1.2. Electrical conductivity

For the two-phase case, we compare our predicted effective electric conductivities of $\text{Al}_2\text{O}_3/\text{Y-TZP}$ composite materials with the measurements by Sanchez-Herencia et al. [42]. Fig. 20 shows the results of effective electric conductivity versus volume fraction of Al_2O_3 for single-layer composites. The electric conductivities of the Al_2O_3 and Y-TZP components used in the simulations are 3.7×10^{-7} and $1.0 \times 10^{-2} \text{ S/cm}$, respectively [42]. When we use a logarithmic scale for the y-axis, the effective electric conductivity exhibits a nearly bi-linear trend, with the intersecting point falling around the point where the volume fraction of Al_2O_3 is 0.8. Before the intersecting point, the effective electric conductivity decreases with the volume fraction of Al_2O_3 at a low rate, whereas after the point, the rate of decrease becomes much steeper. Such a trend is consistent with the previous report [42]. Unlike the previous predictions [279] however, the change of the effective conductivity is smooth and continuous with no singular point, making more physical sense. Our predictions agree well also with the experimental data when the Al_2O_3 volume fraction is below 0.8, yet the predictions are much greater than the measured values once the Al_2O_3 volume fraction approaches 0.9. The reason for the discrepancy, as pointed out in Ref. [279], might lie in the systematic error of the experimental equipment or the lacunae existing in the materials.

4.1.3. Dielectric permittivity

Consider a glass porous structure, either dry or saturated fully by a liquid, i.e., a two-phase case. Sen et al. measured the dielectric constant of such porous systems in three cases: dry, water-saturated and Methanol-saturated [280]. We reproduce the porous structures by QSGS [17] with $c_d = 0.01 \phi_{\text{glass}}$ on 200×200 grids and calculate the effective dielectric constant by LBM with the

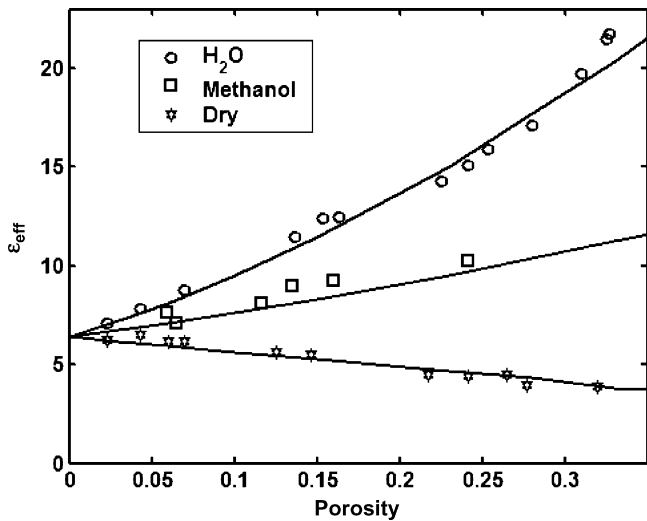


Fig. 21. Effective dielectric permittivity versus porosity for porous glass (two-phase cases) where $c_d = 0.01\phi^{\text{glass}}$, $\epsilon_r^{\text{water}} = 80$, $\epsilon_r^{\text{Methanol}} = 30$, $\epsilon_r^{\text{air}} = 1$, and $\epsilon_r^{\text{glass}} = 6.4$. The symbols are the experimental data [280], and the lines the predicted results.

component dielectric properties: $\epsilon_r^{\text{water}} = 80$, $\epsilon_r^{\text{Methanol}} = 30$, $\epsilon_r^{\text{air}} = 1$, and $\epsilon_r^{\text{glass}} = 6.4$ [280]. Fig. 21 shows the predicted effective dielectric constant versus the porosity for the three cases, compared with the experimental data. The symbols represent the experimental data [280] and the solid lines are the predicted values. The numerical results show good agreements with the experimental data.

When the solid porous structure is partially saturated by a liquid, the effective dielectric constant of the multiphase system may change greatly with the liquid content. A technique has been developed by which the volumetric water content can be evaluated from the measured value of effective dielectric constant of the unsaturated soil sample [165,179,281,282]. Here we simulate such a three-phase system using the present numerical methods. Fig. 22 compares our predicted effective dielectric constant of such unsaturated soil with the measured data of Andisoil (Miyazaki) [169] and those by other theoretical models reported in Refs. [179,182]. The solid soil particles are reproduced by QSGS with

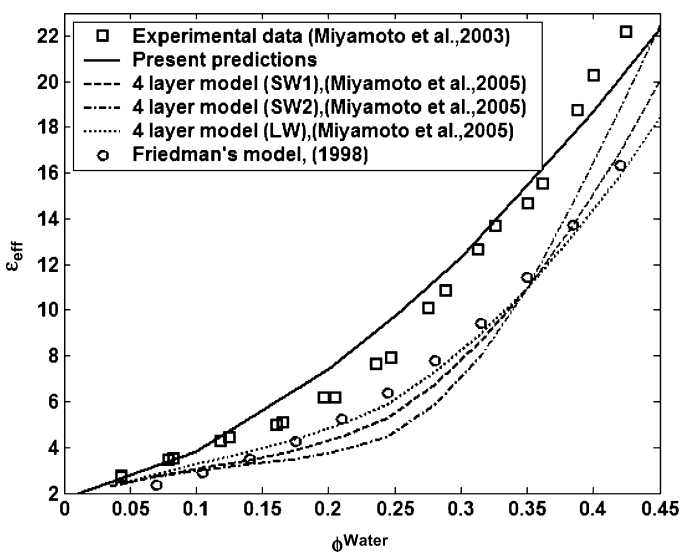


Fig. 22. Effective dielectric permittivity versus volumetric water content for unsaturated soil (three-phase cases) where $\epsilon_r^{\text{water}} = 80$, $\epsilon_r^{\text{soil}} = 5.5$, $\epsilon_r^{\text{air}} = 1$.

$P^{\text{soil}} = 0.27$ and $c_d = 0.01P^{\text{soil}}$. The component dielectric properties used are $\epsilon_r^{\text{water}} = 80$, $\epsilon_r^{\text{soil}} = 5.5$, $\epsilon_r^{\text{air}} = 1$ [182]. Comparing with the results by other theoretical models, the present predictions agree most closely with the experimental data. The agreements should be better if we know the internal geometry in more detail so as to use closer geometrical parameters in QSGS.

4.1.4. Elastic moduli

The theoretical models are more widely used in calculations of mechanical elastic moduli of multiphase materials. Very little effort however has been made for a completely numerical modeling of effective moduli, to the best of the authors' knowledge. Since the displacement field under the pure elastic deformation can also be governed by Eq. (15) under certain assumptions listed in Section 3.2.1, the same methodology can be extended to the estimation of the effective elastic moduli.

First the equivalent microstructures need to be reproduced based on the experimental information. For instance, Tilbrook et al. [283] provided a series of microstructural images of alumina epoxy composite samples. Pores are clearly observable in the composites, although the porosity details are not reported. Their results show roughly that the porosity decreases with the alumina volume fraction $\phi^{\text{Al}_2\text{O}_3}$ when $\phi^{\text{Al}_2\text{O}_3} \geq 50\%$ but increase with $\phi^{\text{Al}_2\text{O}_3}$ otherwise. Since it is reported in the study that the porosity was at most 5% in the Al_2O_3 -Epoxy composites, we propose here a bilinear relationship between the porosity and the volume fraction of alumina:

$$\epsilon = \begin{cases} 0.1 \cdot \phi^{\text{Al}_2\text{O}_3} & (v_f^{\text{Al}_2\text{O}_3} < 50\%) \\ 0.1 \cdot (1 - \phi^{\text{Al}_2\text{O}_3}) & (v_f^{\text{Al}_2\text{O}_3} \geq 50\%) \end{cases} \quad (9')$$

Fig. 23 shows six generated random microstructures of such Al_2O_3 -Epoxy-Pore composites using our approach on a 200×200 grid system, where the light phase is alumina, the grey phase is epoxy, and the dark spots are pores. Compared with the microstructure images of the actual composites (see Fig. 1 in Tilbrook et al.'s paper [283]), the generated ones here capture well the structural details and the stochastic characteristics.

Fig. 24 provides the predicted effective Young's modulus compared with the experimental data of Tilbrook et al. [283]. The properties of alumina and epoxy are listed in Table 3. The elastic properties of the pores are assigned to a small value, such as 10^{-5} GPa. For such a large contrast in the elastic moduli between the two solid components ($E^{\text{Al}_2\text{O}_3} : E^{\text{epoxy}} = 390 : 3.4$), the HS bounds, calculated by Eqs. (3)–(7), failed to provide tight constraints, whereas the present method still yields accurate predictions, without resorting to any empirical parameters. If the porosity data were given, the prediction accuracy could be further improved.

When the direction of the external force and the displacement varies from normal to parallel to the top surface, the same governing equation Eq. (15) is still roughly valid under the assumptions listed in Section 3.2.1 to describe the small shear displacement with varying local shear modulus of composite materials. Fig. 25 shows the predicted effective shear modulus of the alumina-epoxy composites versus the alumina volume

Table 3
Elastic properties of composite materials

Property	Al_2O_3	Epoxy
E (GPa)	390	3.4
K (GPa)	260	3.8
G (GPa)	156	1.26

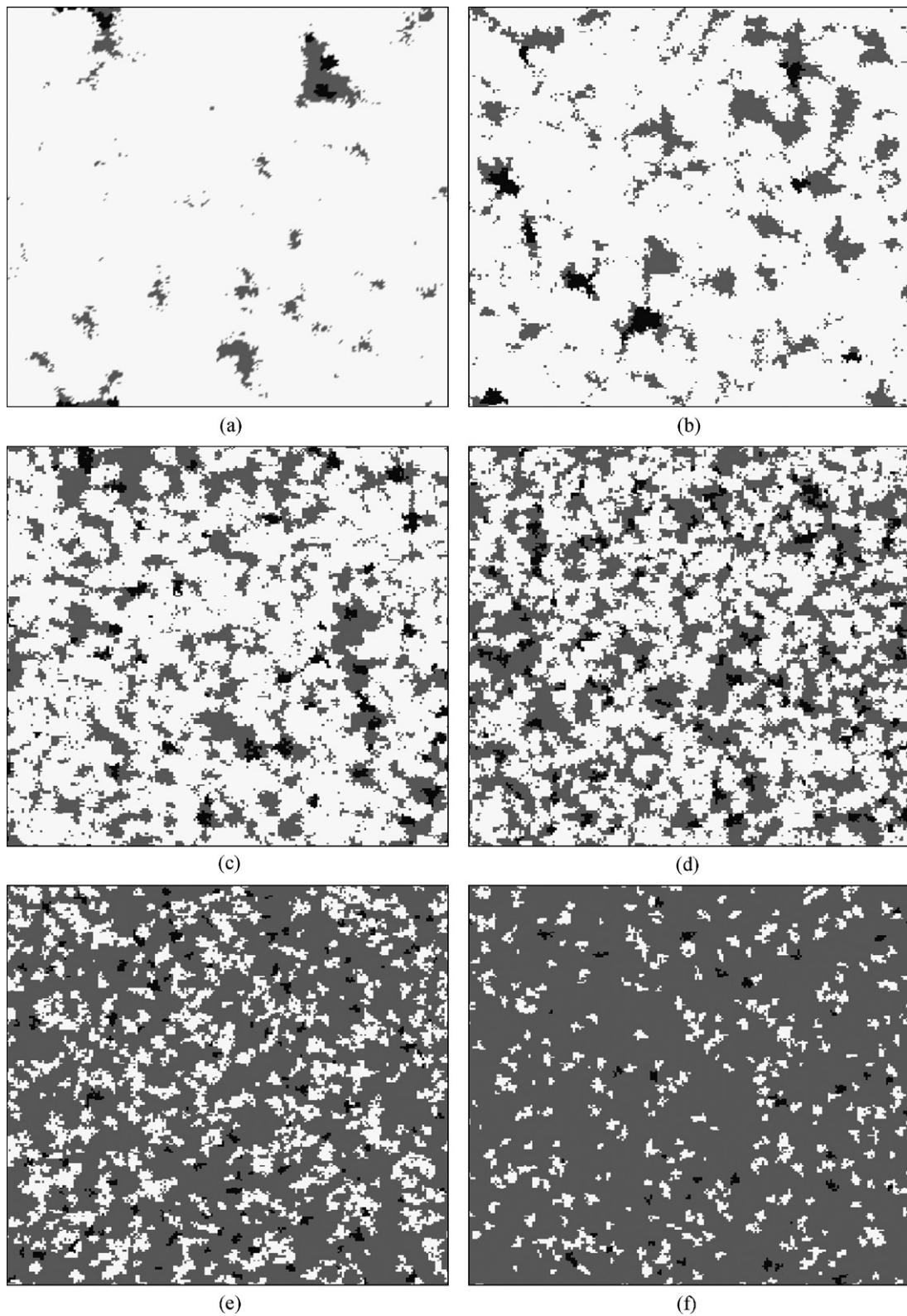


Fig. 23. Reproduced three-phase microstructures of alumina–epoxy composites with pores inside. The parameters used are $c_d^{\text{Al}_2\text{O}_3} = 0.1 \cdot \phi^{\text{Al}_2\text{O}_3} (1 - \phi^{\text{Al}_2\text{O}_3})$ and $c_d^{\text{pore}} = (1 - \phi^{\text{Al}_2\text{O}_3}) \cdot c_d^{\text{Al}_2\text{O}_3}$ for $\phi^{\text{Al}_2\text{O}_3} \geq 50\%$ or $c_d^{\text{pore}} = \phi^{\text{Al}_2\text{O}_3} \cdot c_d^{\text{Al}_2\text{O}_3}$ for $\phi^{\text{Al}_2\text{O}_3} < 50\%$. The light phase is alumina, the grey phase is epoxy and the dark spots are pores. (a) 95% Alumina, 0.5% pore. (b) 85% Alumina, 1.5% pore. (c) 70% Alumina, 3% pore. (d) 55% Alumina, 4.5% pore. (e) 25% Alumina, 2.5% pore. (f) 10% Alumina, 1.0% pore.

fraction for the same three-phase microstructures above. The used shear moduli of Al_2O_3 and epoxy are listed in Table 3. Again with the dispersed pores/voids considered, the predicted effective shear modulus of the Al_2O_3 –epoxy composites are

consistent with the experimental measurements [283]. After the Young's moduli and the shear moduli were calculated, the Poisson's ratio was also calculated and compared with the experimental data [265].

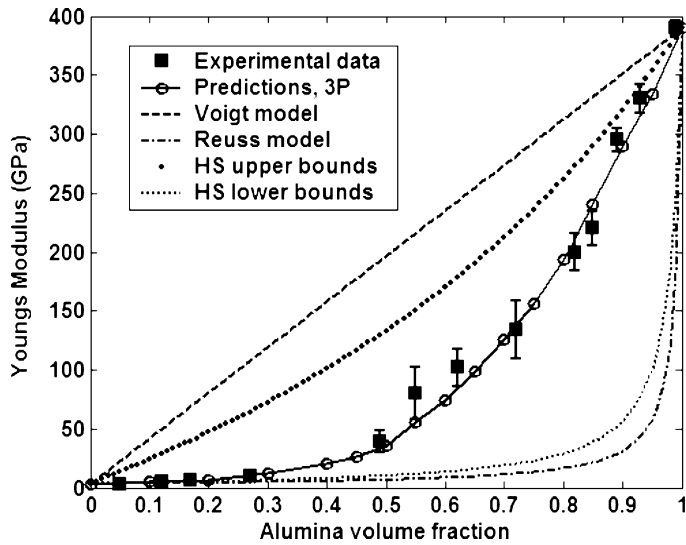


Fig. 24. Comparisons of three-phase (Epoxy, Al_2O_3 , air) predictions of effective Young's Modulus, as a function of alumina volume fraction, for epoxy– Al_2O_3 composites with experimental data [283] and various theoretical modeling results.

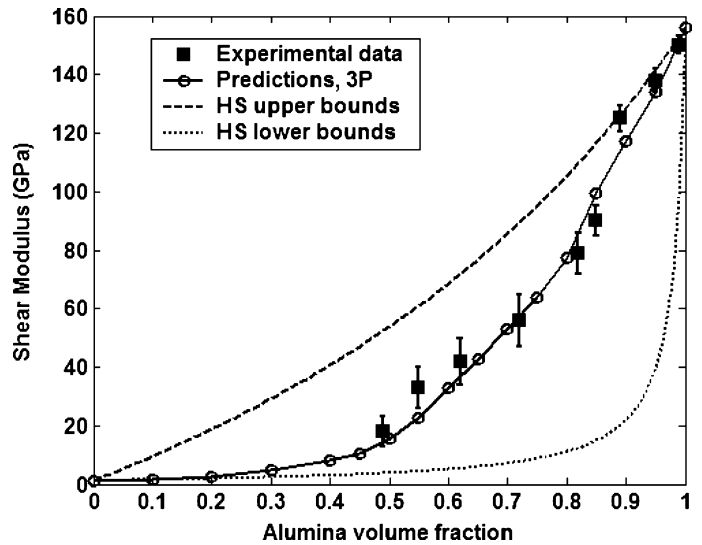


Fig. 25. Predicted effective shear modulus as a function of alumina volume fraction for Al_2O_3 –epoxy composites compared with the experimental data [283] and HS bounds.

4.2. The size effects

Size or scale effect is a prevalent phenomenon in material properties, i.e., many properties thought to be intrinsic turn out to vary when the material dimension is altered. The most striking example was given by Griffith [11] in his famous plot of the experimental data of material strength against its diameter, thus the birth of the fracture mechanics. This discovery of strength-sample size connection was also reported in 1926 by Peirce [12] after he examined the “weakest link” theorem using the testing data on yarn strength. Such size or scale effect have led to related studies on material mechanical [284,285] and other properties [87,130,286,287].

Several researchers have reported that the effective thermal conductivities of porous media may vary for different average pore/particle sizes by their experiments even though the components and the porosities of the media are same [286,288–290]. For the solid–air porous system, finer solid particles often led to a higher effective thermal conductivity at the same porosity [286,290]. The existing theoretical models can hardly explain this

phenomenon, and few analyses have been found to explore the mechanism.

Here we control the average pore/particle size by changing the values of c_d . Based on the definition of c_d in Section 3.1.3, a greater value of c_d leads to a smaller average size of pores/particles at a given porosity ε . Fig. 26 demonstrates two generated structures at $\varepsilon = 0.5$, where (a) has a ten times higher c_d than (b). The structure for a higher c_d looks more uniform and has a higher surface-to-volume ratio. The rough surfaces of the generated structure appear to be typical of natural granular porous media. These complexities of structure may exhaust the computational resources of classical PDE solvers, but have little effect on the computational efficiency of the LBM calculations.

Based on the porous structures generated for different values of c_d , the particle size effect on the effective properties of porous media has been investigated using the present method [17]. To highlight the point without repeating the contents above, we used a general property below to focus on the scale effect.

For the granular solid particle materials, Fig. 27 shows the calculated effective properties versus the solid volume fraction for

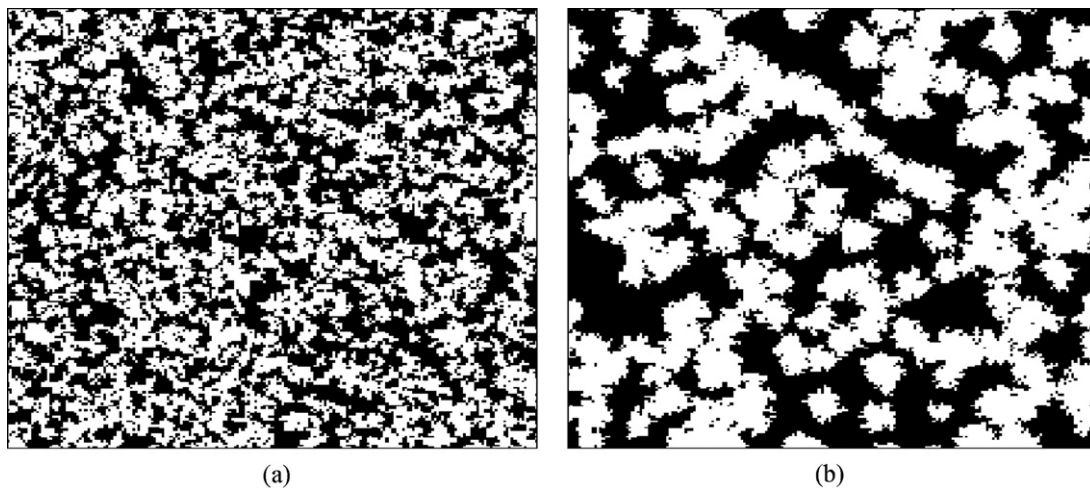


Fig. 26. Isotropic structures for different values of c_d at a same porosity $\varepsilon = 0.5$. The dark is gas and the white is solid. (a) $c_d = 0.1\varepsilon$ and (b) $c_d = 0.01\varepsilon$.

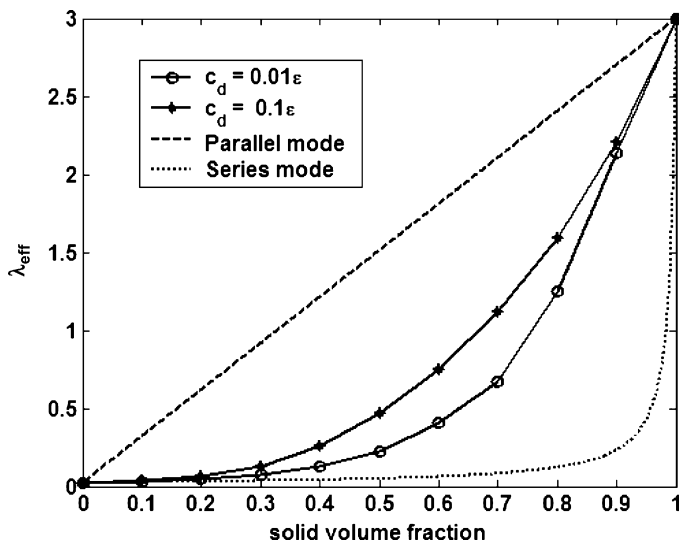


Fig. 27. The predicted effective property versus solid volume fraction for different values of c_d .

two different values of c_d . Suppose the solid particles have a higher value of the property at $\lambda_s = 3.0$ and the property of the other phase is much lower $\lambda_g = 0.025$. No unit is specified here since it depends on the physical type. The theoretical solutions for Parallel mode and Series mode are also provided in the same figure. The results show that this effective property of the random porous media lays in between the values of Parallel mode and Series mode, and a larger average particle size leads to a lower effective property over the full range of the porosity except at 0 and 1. The largest difference between the results of the effective property at different values of c_d occurs where the solid volume fraction is somewhere within 0.5–0.8. Thus, we keep the solid volume fraction at 0.5 and change the value of c_d . The predicted effective properties for different values of c_d are then shown in Fig. 28, which indicates that the effective property increases with the core distribution probability. Since the particle average volume is inversely proportional to the value of c_d , the result means the effective property of granular solid porous media decreases monotonically with the particle average size.

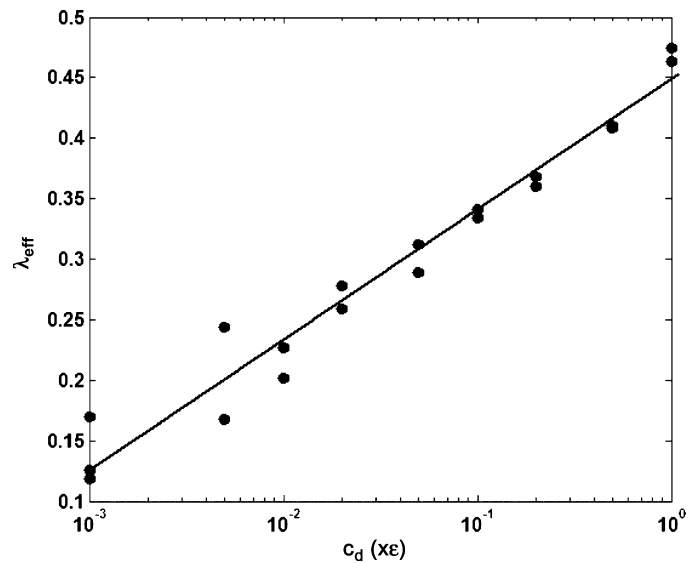


Fig. 28. The predicted effective property versus value of c_d at $\varepsilon = 0.5$.

To explain why a smaller average particle size leads to a higher effective property of porous media, the predicted *potential fields* for two different structures are shown in Fig. 29. For a homogeneous material, as the top and bottom boundaries are both isothermal, the potential contours should be a series of uniform and parallel lines. However, the temperature contours in the porous materials will be distorted by the heterogeneous phase distributions in the materials, as shown in Fig. 29. Still we find that a larger value of c_d results in smoother potential contours which are closer to those for homogeneous materials. Based on the uniformity principle of potential gradient [291,292], the porous structure with a finer particle size generated by a larger value of c_d should lead to a higher effective property.

4.3. Anisotropy effects

Although materials with directional features are common, most previous work has focused on the isotropic cases, except some studies attempted to bring this property-direction dependence

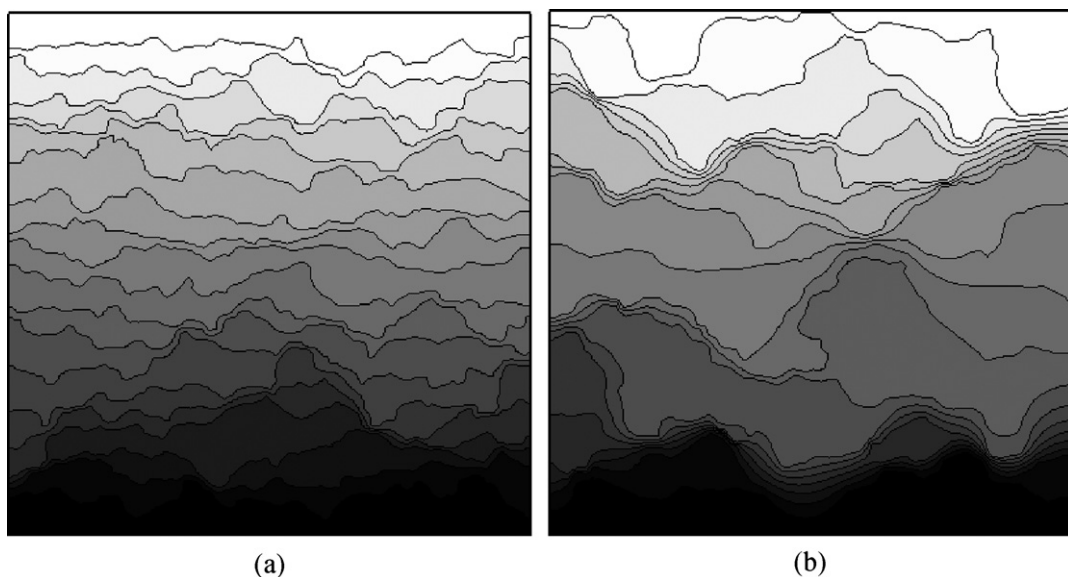


Fig. 29. Potential contours for different values of c_d . (a) $c_d = 0.1\varepsilon$ and (b) $c_d = 0.01\varepsilon$.

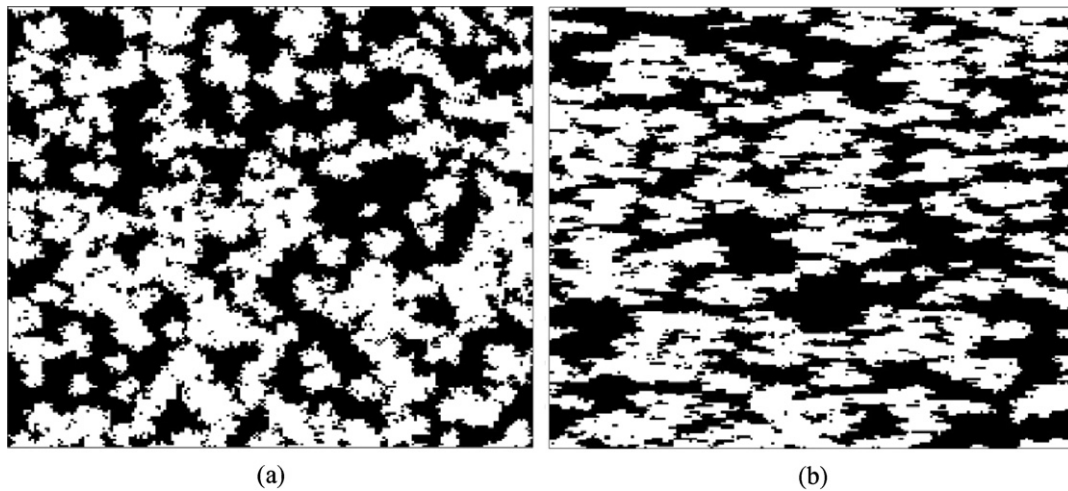


Fig. 30. Microstructures of anisotropic porous media with different directional growth probabilities with $c_d = 0.01$, $\varepsilon = 0.5$. The dark is gas and the white is solid. (a) $D_x:D_y = 1:1$ and (b) $D_x:D_y = 10:1$.

into general formulation [28,49,85,186]. Still a few researchers have generated anisotropic porous materials by using ellipse groups with different axes lengths or orientation angles [193]. Based on the present QSGS process, an anisotropic microstructure can be easily generated by varying values of the directional growth probability, D_i , for the granular porous media. No additional efforts are needed to handle the inter-particle connections. Fig. 30 shows the generated structures for different ratio values of $D_x:D_y$, where D_x is along the horizontal main directions (directions 1 and 3 in Fig. 6) and D_y is the vertical main directions (directions 2 and 4 in Fig. 6). The growth probabilities in the four diagonal directions are always set as a quarter of the minimum value of those in the main directions. The other parameters are $c_d = 0.01$ and $\varepsilon = 0.5$, and the grid used is 200×200 . The generated microstructures show quite different characteristics for different values of directional growth probabilities. The anisotropy increases with the $D_x:D_y$ ratio. The directional growth probabilities are determined based on the macrostructure statistical information, and can thus be estimated by the measurement data from actual porous structures.

After the anisotropic microstructures are generated with the $D_x:D_y$ ratio varying from 0.01 to 100, we predict the effective properties along the y -direction. Fig. 31 shows the numerical results where $\varepsilon = 0.5$, $c_d = 0.01\varepsilon$, $\lambda_s = 3.0$, and $\lambda_g = 0.025$. The results indicate that the effective properties along the y -direction decrease monotonically with the $D_x:D_y$ ratio. For a given porosity, the effective property is enhanced along the direction with higher growth probability, and meanwhile weakened along the direction with lower growth probability.

Another typical anisotropic structure is the aligned fiber material. The two-dimensional two-phase fibrous structures have been studied, for instance, by changing the orientation angle bounds of fibers [214]. Generally, the effective properties of fibrous material would be enhanced along the alignment direction and weakened along the perpendicular direction.

4.4. Morphology effects

The morphology here refers to the internal structural features of a material. For random microstructures, there are at least three typical structure types: granular, fibrous, and netlike. For different structure types, the effective properties usually differ drastically even for the same components and fractions. Due to the complexity of the problem, very few researches have focused on the morphology effect on the effective properties, especially, via

theoretical approaches. Tekce et al. [293] measured the thermal conductivity of copper reinforced polymer composites with different filler shapes and found that the fiber shape may lead the better conductivities than the sphere and plate shapes at the same filler fractions. Since the random generation-growth method can reproduce all the three different types of microstructures, the present mesoscopic method provides a way to study such effects.

Consider two-dimensional two-phase materials with different morphologies reproduced using the random generation-growth method on a 200×200 grid for different dispersed component volume fractions. Again a nominal property without any unit is used here. The component property for the dispersed phase is set at 100 units and that for the continuous phase at 1 unit. The effective properties for the three random microstructures are compared with the theoretical bounds as well as those of a structured sphere array in Fig. 32. The results indicate that (i) the effective properties of the sphere array case are almost the same as the HS lower bounds, for there are no contacts between the dispersed particles in both cases; (ii) the granular structure leads to the lowest

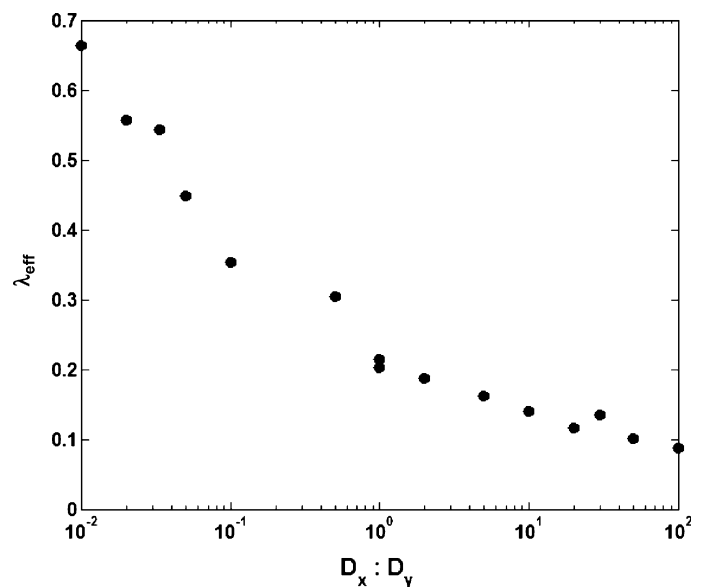


Fig. 31. The predicted effective property of anisotropic porous media for different directional growth probabilities.

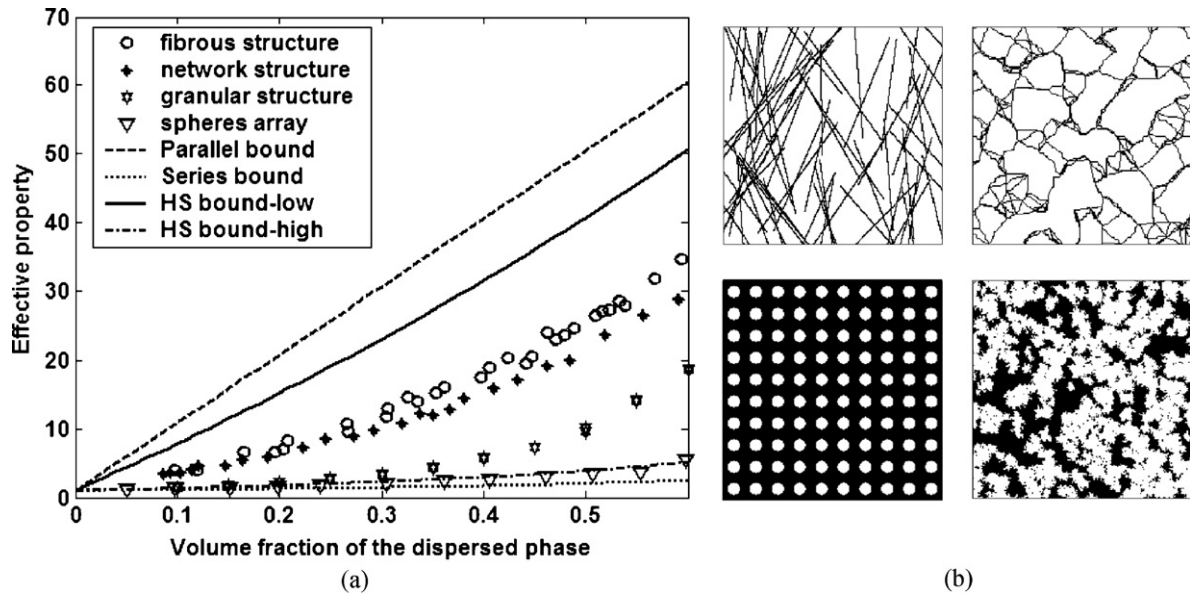


Fig. 32. The effective properties versus volume fractions of the dispersed phases for different morphologies. (a) All structures are assumed isotropic. For the spheres array, 10×10 spheres were used; for the granular structure, $c_d = 0.01\phi^2$; for the netlike structure, $n_{node} = 4$; for the fibrous structure, the fiber's length is set 100 grid size, the width is 1. (b) Schematics of the four structures. For fibrous and netlike structures the dark is solid (dispersed phase); for array and granular random structures the white is the solid.

properties for the same dispersed phase volume fraction. Without considering the contact resistance and connect manner, the fibrous structure seems to be the optimal one for the highest properties. Such results may have important significances for material or structure designs.

4.5. Phase interaction effects

When a porous medium contains more than two phases of state, the effect of the inter-phase interactions on the material properties should be evaluated. For a three-phase porous system involving gas, liquid and solid, the simplest case is to generate the liquid phase using the QSGS tool with a uniform phase interaction growth probability, i.e., $I_i^{l,l} : I_i^{l,s} = 1$ with l representing the liquid phase and s the solid phase. This hypothesis is based on a wetting process characterized by a strong liquid–solid attractive potential, and will result in a uniform liquid film attached on the solid grains as shown in Fig. 33a. The smaller the $I_i^{l,l} : I_i^{l,s}$ ratio, the more uniform is the liquid film (see Fig. 33b). Such structures can be found in certain multi-components composite materials [201]. However, for the unsaturated sandstones or glass assemblies, the wetting characteristic of water is different. Both the lowest interface energy law [211] and the measured images [205] have shown that the water in sandstones or glass assemblies tends to be in aggregation rather than in continuous thin films on the solid surfaces due to the weak wetting properties. Here we reproduce the water distributions similar to those in sandstones by changing the values of $I_i^{l,l} : I_i^{l,s}$ ratio as shown in Fig. 33c and d. Fig. 33 compares the water distributions in the porous media for different phase interaction growth probabilities. In all these cases, the solid phase distributions are isotropic, with volume fraction $\varepsilon = 0.5$, the core distribution probability $c_d = 0.01\varepsilon$, and water volume fraction 0.25, but the $I_i^{l,l} : I_i^{l,s}$ ratio changes from 10:1 to 1:100. A greater $I_i^{l,l} : I_i^{l,s}$ ratio represents a weaker liquid–solid inter-phase attractive potential and a weaker wetting interface, i.e., the liquid will be more aggregative.

The phase interaction effects on the effective property of multiphase porous media can thus be investigated. Assuming an unsaturated sandstone case where the solid particle volume

fraction is $\phi^s = 0.5$ with $c_d = 0.01\phi^s$, the water volume fraction is $\phi^l = 0.3$, and the component properties are $\lambda_s = 3.0$, $\lambda_l = 0.1$, and $\lambda_g = 0.025$ respectively. Fig. 34 shows the predicted effective properties at different liquid–solid phase interaction growth probabilities. The results indicate that the effective property of multiphase porous media increases with the degree of liquid phase conglomeration. The effective property changes little when $I_i^{l,l} : I_i^{l,s} < 1$, and increases remarkably when $I_i^{l,l} : I_i^{l,s} > 10$.

4.6. Examination of the current measurement techniques

When using the numerical method to study the effective properties of multiphase materials in comparison with the existing experimental data, it was interesting to find that for the same problem (i) the two-dimensional predictions were often different from the three-dimensional results; and (ii) some experimental data agreed with the two-dimensional predictions while the others go well with the three-dimensional calculation results.

For instance, Fig. 35 compares the effective thermal conductivities of moist sands in frozen and unfrozen states measured by the hot-probe technique [271,273] with the corresponding predictions by both two- and three-dimensional methods. The parameters are $\varepsilon = 0.52$, $k_s = 2.85$ W/m K, $k_w = 0.594$ W/m K, $k_g = 0.0249$ W/m K, and $k_{ice} = 2.38$ W/m K, all adopted from [272]. The two-dimensional simulations use a 200×200 grid, and the three-dimensional cases use a $60 \times 60 \times 60$ grid for acceptable computational costs. The results show that the experiment data are consistent with the two-dimensional predictions, yet deviate from the three-dimensional predictions. The reason may likely be that the hot-probe or hot-wire technique, which is based on the line heat source and axial symmetric assumption, is essentially a two-dimensional technique.

Carson et al. [294] developed a transient comparative method of a largely 3D technique to measure the effective thermal conductivity of a pseudo-porous food analogue. Fig. 36 shows the experimental data comparing with the respective two-dimensional and three-dimensional predictions using the present models. The parameters are $c_d = 0.01$, $k_s = 0.60$ W/m K, and $k_g = 0.035$ W/m K. Again the two-dimensional simulations use a

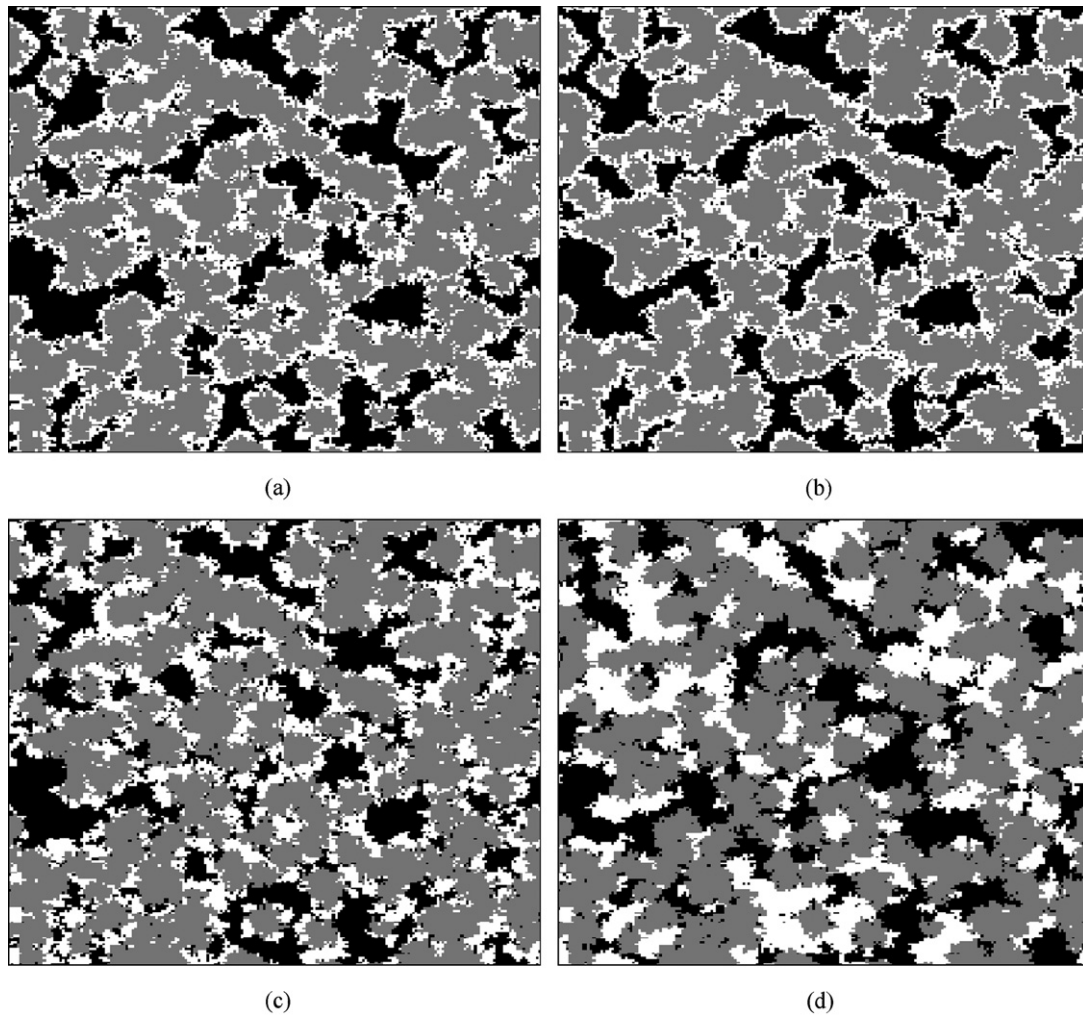


Fig. 33. Microstructures of three-phase porous media with different phase interaction growth probabilities. The gray is solid particles, the white is liquid, and the dark is gas. The solid is isotropic with $c_d = 0.01\epsilon$. The porosity $\epsilon(P_2) = 0.5$, and the liquid volume fraction $P_l = 0.25$. (a) $I_l^{ll} : I_l^{ls} = 1 : 1$. (b) $I_l^{ll} : I_l^{ls} = 1 : 10$. (c) $I_l^{ll} : I_l^{ls} = 10 : 1$. (d) $I_l^{ll} : I_l^{ls} = 100 : 1$.

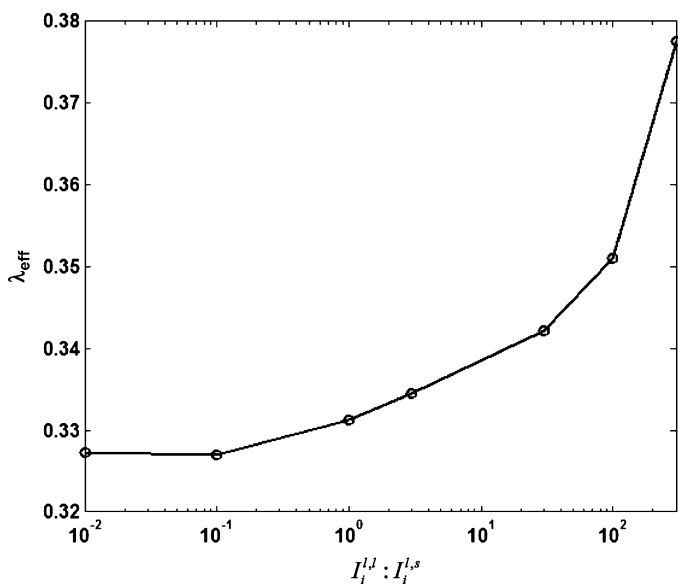


Fig. 34. ETC of three-phase porous media for different liquid–solid phase interaction growth probabilities. The parameters are: $\phi^s = 0.5$, $c_d = 0.01\phi^s$, $\phi^l = 0.3$, $\lambda_s = 3.0$, $\lambda_l = 0.1$, and $\lambda_g = 0.025$.

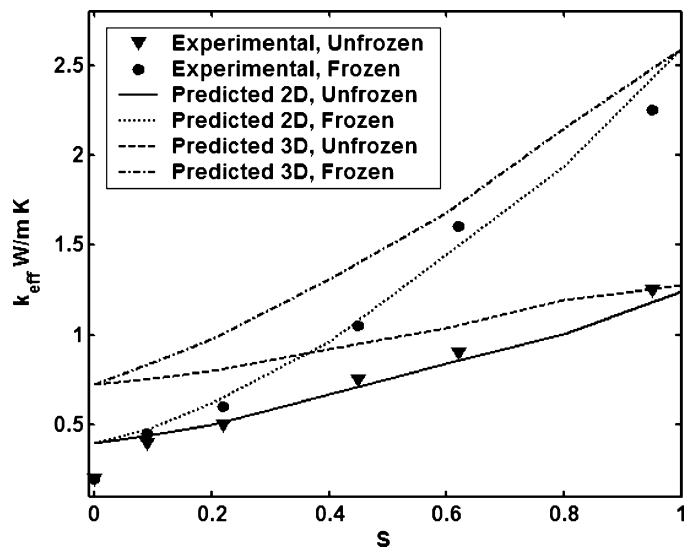


Fig. 35. Comparisons between our numerical predictions with the experimental data of Singh et al. [271] measured by the hot-probe method.

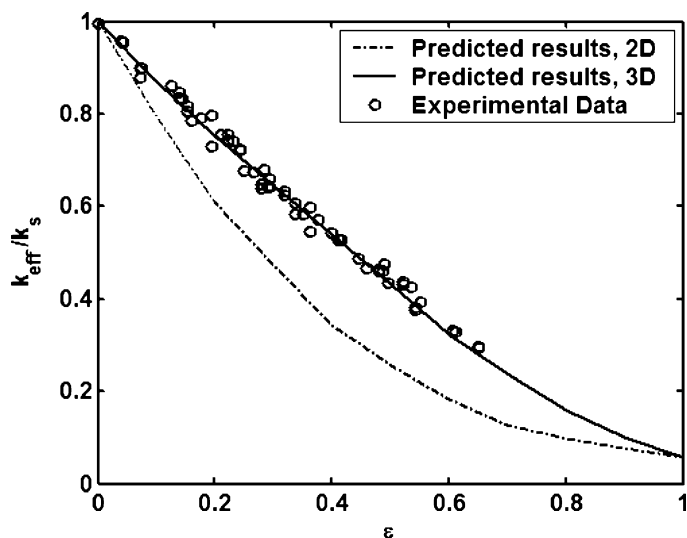


Fig. 36. Comparisons between our numerical predictions with the experimental data of Carson et al. [294] measured by a transient comparative method.

200 × 200 grid and the three-dimensional cases use a 60 × 60 × 60 grid. The three-dimensional predictions agree with the experimental data, while the two-dimensional predictions appear much lower. Although the generated random structures are not exactly same as those in Carson's experiments, which might explain some of the differences [145], this comparison may still serve as evidence to show that Carson's transient comparative method is a three-dimensional measurement technique.

5. Conclusions and perspectives

5.1. Concluding remarks

It has always been one of the most important but challenging goals to establish connections between the effective properties of multiphase materials and their internal microstructures. Inherently, two major issues are involved—the internal morphology of the material formed by the constituents, and the interactions among themselves. However, even for simple cases, bringing these two factors into a theoretical treatment often poses as a challenge. Once materials become more complex with irregular internal morphology and formed by constituents of different phases, prediction of the system behavior turns into a daunting task.

This review first surveys and summarizes the existing major analytical models dealing with the effective property predictions for heterogeneous materials. Besides the classical fundamental models, with or without the modified or added empirical parameters, the combined models and the network schemes of basic models have also attracted much attention in recent years. However, despite quick, often rough, estimation and/or small computation costs, the theoretical models are unable to reflect the effects of connections and interactions of the constituents on the effective properties of multiphase material systems. The capability of each model is largely empirical and the models cannot be used for new material designs.

The numerical methods using computer simulations provide an alternative in dealing with the effective properties of complex multiphase materials. After reviewing the previous numerical methods and summarizing the challenges due to complex geometries and conjugate effects, we highlight the recent progress in the mesoscopic methods that can predict more accurately and efficiently the thermal, electric and mechanical properties of

multiphase materials with complex internal structures. Two major parts are involved: (i) a multi-parameter random generation-growth algorithm for reproducing multiphase microstructures based on the macroscopic statistical information of real structures; (ii) a high-efficiency lattice Boltzmann model for solving the relevant governing equations with conservation and continuity constraints automatically satisfied for a closed system. The theoretical analysis indicates that such numerical methods are applicable to calculate effective thermal conductivity, electrical conductivity, dielectric permittivity and even elastic moduli for stable and equilibrium multiphase systems.

Various applications have validated the feasibility, effectiveness and robustness of the mesoscopic methods by comparing the predictions with existing experimental data for different cases. Since the microstructure reconstructions are controllable by adjusting the statistic parameters, the mesoscopic numerical method has been used to investigate the effects of structure geometries and phase interactions on the effective properties for complex materials. For two-phase systems, the size effect of particles, the anisotropy effect of microstructures and the morphology effect are therefore studied. For multiphase systems, different phase interactions, which influence the aggregations of the liquid phase, are taken into account for the effective properties of materials. By comparisons between the experimental data and the numerical results, the existing experimental techniques are also examined, concluding that the methods based on hot wire or hot probe are all two-dimensional measurement technologies.

It is also shown that for given system composition and structure, this numerical methodology is in essence a model built on sound physics principles with *prior* validity, without resorting to *ad hoc* empirical treatment.

5.2. Some perspectives

Facing such a huge and ever-increasing body of research work in complex materials, one could not help but feeling overwhelmed. So what we have done in this article only offers a glimpse of the subjects discussed, and much remains to be said and done. In this section we make some less restrictive comments, and offer our often still fluidic views and even speculations on the emerging topics down the road.

5.2.1. The local and global scale or size effects

Strictly speaking, the scaling effects discussed in this review respond only to the fact that many material properties are dependent on their physical size or dimensions. In other words, we have only touched upon the influence of the material dimension, and are falling short in reviewing the progresses in developing theories and methodologies aimed to model the full range of the hierarch of different characteristic scales in both space, as well as time. The drastic changes in properties of the same materials at bulk versus at nanoscale are the most striking manifestation of such influence in spatial domain, whereas the specific relativity versus the Newton's Second Law of Motion deals with the issue in temporal terms. In between these extremes, such scale effects still exists, all depending on whether they are negligible for a given problem, in comparison to other factors [102,109,295–313].

For instance, it is well documented and widely known that material strength (especially those of brittle materials) is sensitive to the size of the material tested: the strength increases for a shorter and thinner sample. This kind of scale effect has been demonstrated and modeled by many, including the work described in Section 4.2 of this paper. For convenience, we term this as the *local* scale effect in a limited length range. Furthermore, such a scale effect is clearly not continuous, and increasing evidence has

people believe that the relationship breaks down over large range of scales in that there are often different physical laws dictating the behaviors of the same material at nano-, meso- and macro-scales, a scale effect in *global* scope. As we discussed above, the rapid developments of the microscopy technique enable us to observe and measure more and finer microstructures to realize that they are actually multiscale as well. For example, it has been found that the particles in some granular materials are actually themselves assembles of numerous fine fibers [189,190], as in the cases to predict the effective properties of two-level granular porous media [314].

5.2.2. Nanoscale size effects and multiscale modeling

Needless to say, the multiscale microstructure and modeling its effects on the effective properties of the material are a very important yet challenging topic for materials design.

It is lesser a problem when modeling a system over the range of meso (roughly at 10^{-6} – 10^{-4} m) to macroscale, for nearly all the physical laws are valid at both scales, provided that the *local* size effect is included when necessary. So the main issues in this case have to do with efficiency and accuracy in deciding the modeling approaches: obviously, for one thing, there much more structural details and interactions to account for at meso scale level. Even if there are nanoscale components in a complex system, for modeling at meso scale, we can always using the corresponding effective properties of the nanoscale components without immersing into the details at nanoscales.

Problems lie in the nanoscale arena. It has been reported that, as summarized succinctly by Rajagopal et al. [315,316], that “the surface energy of Ag nanoparticles was found to be significantly higher than the bulk Ag [317]; the size dependence of surface ferromagnetism of Pd fine particles was found only on (1 0 0) facets [318]. Detection of the *N* statistical polarization in a small ensemble of electron spin centers was by magnetic resonance force spectroscopy [319]. An unexpected decrease in the strength of various materials as sizes of microns grains become nanometers was found [320]. A large critical current at nanosizes of superconductors [321] was measured. There are experiments on molecular magnets [322] and possible canted magnetism in Gd clusters [323]. There are also discussions of microelasticity at the nanoscale [324,325]. There are also recent theoretical works dealing with existence of temperature on the nanoscale [326], possible tests of the thermodynamic approach to granular media [327], and scaling relations in equilibrium thermostatics with long range interactions with implications to nanosystems [328]”. More recent additions include the reports on the negative conductance [329], super thermal conductance [330], and the inter-frictionless flow [331] all exhibited by carbon nanotubes. Most of these abrupt changes in properties at the nanoscale are attributed to the quantum phenomena dominant at the scales, and incorporating such influences into a modeling scheme poses a major challenge as new research direction.

More specifically, as stated above, there are limitations of the conventional continuum approaches (e.g., the finite element method) to describe the behavior of materials at scales smaller than tens of micros [299], and such often striking differences in behaviors of the same material at different length scale have prompted development of individual theories for each specific characteristic length. At the present time, a truly seamless multiscale approach for computer simulation is still pending [332], and an expedient way of connecting or transiting between different scales can be carried out by the so-called “hand-shaking” strategy that the *effective* information gained from a lower scale modeling is summed into a finite set of parameters and passed

onto a higher scale so as to cover the scale range from macro, mesoscale to nanoscales [296,297,302,303,305,306].

5.2.3. Scale effect in temporal domain

Obviously, the behaviors of materials are also dictated by the speed or frequency of the external excitations, another formidable dimension adding to the complexity of the problem dealing with the effective properties of complex materials. In general, when the external load is non-static, the effective properties of the materials become a function of time or load changing frequency as well—a problem of material dynamics.

Also, because of the existence of the inertia for materials, it takes time for a material system to reach a stable situation and/or an equilibrium state. In many cases, the transient responses and the non-equilibrium behaviors of the materials are of concern and interest, and have necessitated the different methodologies in tackling such problems, including transient behavior studies [312,333], non-equilibrium analysis [334], material viscoelasticity, time dependent behaviors, and system rheology [335] [336].

5.2.4. Other complexities and bi-modular behaviors

In dealing with certain complex materials know as the soft matters [337] with multiphase composition, porous and highly deformable structures, and often non-equilibrium state, additional issues were illustrated by Pan et al. [338]. Examples include the mathematics in internal structural packing geometry, the affinity issue between macro–micro behaviors, friction, internal energy dissipation and hysteresis, and the allometric or scaling problems existed in such complex materials.

Another peculiar problem is the so-called bi-modular behavior. Anisotropy is responsible for many of the challenges in studying material behaviors. However, even at the same direction, most soft matters behave differently depending on the sign of the force. In other words, the entire stress–strain relationship is quite different in tension versus in compression. At issue are two problems. First, the current theories treating all materials as inherently identical in both compression and tension have to be re-examined. Also, any proposed new model needs to be evaluated to satisfy the following criteria: (1) The tensor matrix of the effective properties must be symmetric in any coordinate systems in order for the system internal energy to be positive definite; (2) The individual values of the properties are restricted in relation to one another such that the matrix itself is positive definite [339–341].

5.2.5. Structural effects, biometrics and metamaterials

Next, we would like to further elucidate how significant the internal structure can be for the behaviors of a material. It has long been recognized that the molecular morphology exerts a direct impact on the macroscopic properties of polymeric materials [296,297]. Such structural influences become all the more obvious for materials with more visible microstructural characteristics such as fibrous assemblies [342], granular [162] and aggregated materials [174,343], and fiber reinforced composites [89,157,186]. Many physical properties (e.g., the elastic constants) of these materials can be adjusted by altering the internal structures [344–349].

Upon realizing this close connection between structure and properties, we start to discover various examples where nature once again demonstrates its brilliance. By possessing a surface with tiny scale hair, many plants and insects acquire high hydrophobicity, or the so-called self-cleaning lotus effects [350–352]. Other examples include the peculiar frictional and adhesive properties as found in gecko and other excellent insect climbers [353–355], and the structure-generated/modulated colors in the natural world [356–359].

A good case, created by human beings, highlighting the importance of the materials internal structure, is the recently emerged metamaterial (or meta material)—a material gains its properties from its structure rather than directly from its composition. The term was coined in 1999 by Walser [100] and defined as “Macroscopic composites having a manmade, three-dimensional, periodic cellular architecture designed to produce an optimized combination, not available in nature, of two or more responses to specific excitation.”

The still more fascinating examples are the so-called metamaterials [4,9,100,360,361]. The first types of such metamaterials include the materials exhibiting negative refraction, also referred to as the left-handed (meta) materials with startling optical properties, non-existent in natural materials [362,363]. In order for its structure to affect electromagnetic waves, a metamaterial must have structural features smaller than the wavelength of the electromagnetic radiation it interacts with. For visible light, which has wavelengths of less than one micrometer typically (560 nanometers for sunlight), the structures are generally half or less than half this size; i.e., less than 280 nm [100].

Another recent case in manipulating the internal structure to achieve unique properties non-existent in nature is the so-called nanostructured materials: nanoscale components are assembled into desirable constructions so that the completed system behaves differently from either its nano components or the same material but in pure bulk form. Such nanostructured materials have attracted wide attention for their huge potential applications and markets [10,307,364,365].

To sum up, one can never emphasize too much the importance of materials to the human civilization. In fact, materials used by human beings at different time periods were often the most credible records left for anthropologists to determine the degree of civilization of the time [366]. So much so that the whole human history is chronicled by the representative material used.

From early time to present, one can see a clear progressive trace of not only the types of the materials used, but also the way they were/or are produced. In the Stone Age, the axes and knives made of rocks were shaped manually by bare hands using other rocks. Then some tools were gradually developed by which wood, earth and bones could be crafted mechanically into useful shapes and forms [366]. Wide use of metals represents a new era where metals can be smelted and reformed thermodynamically into products via phase changes [367]. The proliferation of polymeric materials is resulted from the acquired capacity to synthesize the material chemically at molecular level. Today, with powerful computational capacity and much better understanding and ability in manipulating materials at many levels and scales, new generations of materials, even non-existent in nature, with high functionalities emerge one after another, such as composite materials, functionally gradient materials, metamaterials and nanoscale materials and structures, a triumph of knowledge and creativity. Still the golden age for newer and better materials is yet to arrive and we see no boundary but endless potentials.

Acknowledgements

The present work is supported by the grants from the NTC-M04-CD01. The authors would like to thank Dr. R. Zimmerman, Dr. J. Carson, Dr. K. Bakker and Dr. Z.Y. Guo for helpful discussions, and Dr. Miyamoto and Dr. Carson for providing the experimental data.

References

- [1] C. Burger, B.S. Hsiao, B. Chu, *Annual Review of Materials Research* 36 (2006) 333–368.

- [2] L.E. Fried, M.R. Manaa, P.F. Pagoria, R.L. Simpson, *Annual Review of Materials Research* 31 (2001) 291–321.
- [3] J. Haines, J.M. Leger, G. Bocquillon, *Annual Review of Materials Research* 31 (2001) 1–23.
- [4] C. Rockstuhl, T. Paul, F. Lederer, T. Pertsch, T. Zentgraf, T.P. Meyrath, H. Giessen, *Physical Review B* 77 (2008) 035126.
- [5] R.Y. Umetsu, K. Kobayashi, A. Fujita, R. Kainuma, K. Ishida, K. Fukamichi, A. Sakuma, *Physical Review B* 77 (2008) 104422.
- [6] E.B. Wei, G.Q. Gu, Y.M. Poon, *Physical Review B* 77 (2008) 104204.
- [7] S. Weiner, H.D. Wagner, *Annual Review of Materials Science* 28 (1998) 271–298.
- [8] R.P. Wool, *Soft Matter* 4 (2008) 400–418.
- [9] Y. Wu, Y. Lai, Z.Q. Zhang, *Physical Review B* 76 (2007) 205313.
- [10] A.C. Balazs, *Current Opinion in Solid State & Materials Science* 7 (2003) 27–33.
- [11] A. Griffith, *Philosophical Transactions of the Royal Society A* 221 (1920) 163–198.
- [12] F.T. Peirce, *Journal of the Textile Institute* 17 (1926) T355–T368.
- [13] C.M. Bishop, M. Tang, R.M. Cannon, W.C. Carter, *Materials Science Engineering a—Structural Materials Properties Microstructure and Processing* 422 (2006) 102–114.
- [14] S.L. Bryant, K.E. Thompson, *Current Opinion in Colloid & Interface Science* 6 (2001) 217–222.
- [15] H.K. Lee, S.H. Pyo, *Composites Science and Technology* 68 (2008) 387–397.
- [16] H.Y. Sun, N. Pan, *Composite Structures* 74 (2006) 25–29.
- [17] M.R. Wang, J.K. Wang, N. Pan, S.Y. Chen, *Physical Review E* 75 (2007) 036702.
- [18] Z.Y. Fan, *Philosophical Magazine a—Physics of Condensed Matter Structure Defects and Mechanical Properties* 73 (1996) 1663–1684.
- [19] A.A. Gusev, *Advanced Engineering Materials* 9 (2007) 117–120.
- [20] A. Bhattacharya, V.V. Calmidi, R.L. Mahajan, *International Journal of Heat and Mass Transfer* 45 (2002) 1017–1031.
- [21] V.V. Calmidi, *Transport phenomena in high porosity metal foams*, in: Department of Mechanical Engineering, vol. Ph.D, University of Colorado, Boulder, 1998.
- [22] V.V. Calmidi, R.L. Mahajan, *Journal of Heat Transfer—Transactions of the Asme* 121 (1999) 466–471.
- [23] E.N. Schmierer, A. Razani, *Journal of Heat Transfer—Transactions of the Asme* 128 (2006) 1194–1203.
- [24] W.H. Tao, H.C. Hsu, C.C. Chang, C.L. Hsu, Y.S. Lin, *Journal of Cellular Plastics* 37 (2001) 310–332.
- [25] J.W. Wu, W.F. Sung, H.S. Chu, *International Journal of Heat and Mass Transfer* 42 (1999) 2211–2217.
- [26] N. Pan, *Physics of Fibrous Soft Matters*, Higher Education Publishing, Inc., Beijing, 2005.
- [27] N. Djilali, *Energy* 32 (2007) 269–280.
- [28] J.G. Pharoah, K. Karan, W. Sun, *Journal of Power Sources* 161 (2006) 214–224.
- [29] M.J. Biercuk, M.C. Llaguno, M. Radosavljevic, J.K. Hyun, A.T. Johnson, J.E. Fischer, *Applied Physics Letters* 80 (2002) 2767–2769.
- [30] Y.M. Chen, J.M. Ting, *Carbon* 40 (2002) 359–362.
- [31] S.U.S. Choi, Z.G. Zhang, W. Yu, F.E. Lockwood, E.A. Grulke, *Applied Physics Letters* 79 (2001) 2252–2254.
- [32] F. Frusteri, V. Leonardi, G. Maggio, *Applied Thermal Engineering* 26 (2006) 1883–1892.
- [33] F. Frusteri, V. Leonardi, S. Vasta, G. Restuccia, *Applied Thermal Engineering* 25 (2005) 1623–1633.
- [34] X.Q. Gao, Q.G. Guo, J.L. Shi, G.S. Li, J.R. Song, L. Liu, *New Carbon Materials* 20 (2005) 18–22.
- [35] M. Lutz, R. Zimmerman, *Journal of Thermal Stresses* 19 (1996) 39–54.
- [36] Y. Miyamoto, W.A. Kaysser, B.H. Rabin, A. Kawasaki, R.G. Ford, *Functionally Graded Materials: Design, Processing, and Applications*, Kluwer Academic Publishers, Boston, 1999.
- [37] G.H. Paulino, Z.H. Jin, J.R.H. Dodds, in: B. Karahaloo, W.G. Knauss (Eds.), *Comprehensive Structural Integrity*, vol. 2, Elsevier Science, Amsterdam, 2003, pp. 607–644.
- [38] M. Lutz, R. Zimmerman, *International Journal of Solids and Structures* 42 (2005) 429–437.
- [39] N. Araki, D.W. Tang, A. Ohtani, *International Journal of Thermophysics* 27 (2006) 209–219.
- [40] E.M. Carrillo-Heian, R.D. Carpenter, G.H. Paulino, J.C. Gibeling, Z.A. Munir, *Journal of the American Ceramic Society* 84 (2001) 962–968.
- [41] A.H. Wu, W.B. Cao, C.C. Ge, J.F. Li, A. Kawasaki, *Materials Chemistry and Physics* 91 (2005) 545–550.
- [42] A.J. Sanchez-Herencia, R. Moreno, J.R. Jurado, *Journal of the European Ceramic Society* 20 (2000) 1611–1620.
- [43] X.H. Zhu, Q. Wang, Z.Y. Meng, *Journal of Materials Science Letters* 14 (1995) 516–518.
- [44] K. Eguchi, T. Hoshino, T. Fujihara, in: B. Iltschner, N. Cherradi (Eds.), *Third International Symposium on Structural Functional Gradient Materials Proceedings of FGM'94*, Presses Polytech. Univ. Romandes, Lausanne, Switzerland, (1995), pp. 619–625.
- [45] M. Niino, M. Koizumi, in: B. Iltschner, N. Cherradi (Eds.), *Third International Symposium on Structural Functional Gradient Materials Proceedings of FGM'94*, Presses Polytech. Univ. Romandes, Lausanne, Switzerland, (1995), pp. 601–605.
- [46] K.A. Khor, Y.W. Gu, *Thin Solid Films* 372 (2000) 104–113.
- [47] K.A. Khor, Y.W. Gu, Z.L. Dong, *Surface & Coatings Technology* 139 (2001) 200–206.
- [48] A. Bouguerra, *Journal of Physics D—Applied Physics* 32 (1999) 2797–2803.
- [49] S.P. Friedman, S.B. Jones, *Water Resources Research* 37 (2001) 2929–2942.

- [50] R. Knight, A. Abad, *Geophysics* 60 (1995) 431–436.
- [51] C. Li, P. Tercier, R. Knight, *Water Resources Research* 37 (2001) 1783–1793.
- [52] J.Y. Lou, S. Harrington, D.M. Zhu, *Physical Review E* 60 (1999) 5778–5782.
- [53] L.S. Verma, A.K. Shrotriya, R. Singh, D.R. Chaudhary, *Journal of Physics D—Applied Physics* 24 (1991) 1515–1526.
- [54] J.C. Geminard, H. Gayvallet, *Physical Review E* 64 (2001) 041301.
- [55] Q.Z. Chen, S.E. Harding, N.N. Ali, A.R. Lyon, A.R. Boccaccini, *Materials Science & Engineering R—Reports* 59 (2008) 1–37.
- [56] D. Williams, *Biomaterials* 29 (2008) 1737–1738.
- [57] R. Kumar, D. Liu, L. Zhang, *Journal of Biobased Materials and Bioenergy* 2 (2008) 1–24.
- [58] R. Vasita, K. Shanmugam, D.S. Katti, *Current Topics in Medicinal Chemistry* 8 (2008) 341–353.
- [59] F. Barrere, T.A. Mahmood, K. de Groot, C.A. van Blitterswijk, *Materials Science & Engineering R—Reports* 59 (2008) 38–71.
- [60] M. Cazacu, A. Vlad, G. Munteanu, A. Airinei, *Journal of Polymer Science Part A—POLYMER Chemistry* 46 (2008) 1862–1872.
- [61] J. Gegner, *Materialwissenschaft Und Werkstofftechnik* 39 (2008) 33–44.
- [62] K. Herve, O. Cadot, S. Golhen, L. Ouahab, J. Yamada, *Research on Chemical Intermediates* 34 (2008) 191–199.
- [63] G.R. Whittell, I. Manners, *Advanced Materials* 19 (2007) 3439–3468.
- [64] D. Maspoch, D. Ruiz-Molina, J. Veciana, *Chemical Society Reviews* 36 (2007) 770–818.
- [65] S. Mormet, C. Elissalde, O. Bidault, F. Weill, E. Sellier, O. Nguyen, M. Maglione, *Chemistry of Materials* 19 (2007) 987–992.
- [66] X.G. Hu, S.J. Dong, *Journal of Materials Chemistry* 18 (2008) 1279–1295.
- [67] T.M. Osman, *Jom* 60 (2008) 14–17.
- [68] S.V. Bobylev, I.A. Ovid'ko, *Reviews on Advanced Materials Science* 17 (2008) 76–89.
- [69] X. Feng, C.L. Peng, H.X. Lu, *Progress in Chemistry* 20 (2008) 273–279.
- [70] T.J. Huang, *MRS Bulletin* 33 (2008) 226–231.
- [71] P. Rodgers, *Nature Nanotechnology* 3 (2008) 76.
- [72] J.C. Crocker, *Nature* 451 (2008) 528–529.
- [73] V.S. Arunachalam, E.L. Fleischer, *MRS Bulletin* 33 (2008) 261–263.
- [74] B. Hayman, J. Wedel-Heinen, P. Brondsted, *MRS Bulletin* 33 (2008) 343–353.
- [75] B. Raj, M. Vijayalakshmi, P.R.V. Rao, K.B.S. Rao, *MRS Bulletin* 33 (2008) 327–337.
- [76] G.P. Smestad, *Solar Energy Materials and Solar Cells* 92 (2008) 521.
- [77] M.S. Whittingham, *MRS Bulletin* 33 (2008) 411–419.
- [78] D.M. Wood, N.W. Ashcroft, *Philosophical Magazine* 35 (1977) 269–280.
- [79] J.E. Lugo, J.A. del Rio, J. Taguena-Martinez, *Solar Energy Materials and Solar Cells* 52 (1998) 239–249.
- [80] A.G. Marinopoulos, V. Vitek, J.L. Bassani, *Physica Status Solidi a—Applied Research* 166 (1998) 453–473.
- [81] R. Masson, M. Bornert, P. Suquet, A. Zaoui, *Journal of the Mechanics and Physics of Solids* 48 (2000) 1203–1227.
- [82] V.A. Buryachenko, N.J. Pagano, *Mathematics and Mechanics of Solids* 8 (2003) 403–433.
- [83] Z.H. Li, C. Wang, C.Y. Chen, *Computational Materials Science* 27 (2003) 381–392.
- [84] Y.J. Liu, X.L. Chen, *Mechanics of Materials* 35 (2003) 69–81.
- [85] M.G. Forest, X.Y. Zheng, R.H. Zhou, Q. Wang, R. Lipton, *Advanced Functional Materials* 15 (2005) 2029–2035.
- [86] A. Borbely, P. Kenesei, H. Biermann, *Acta Materialia* 54 (2006) 2735–2744.
- [87] H. Le Quang, Q.C. He, *Journal of the Mechanics and Physics of Solids* 55 (2007) 1899–1931.
- [88] S.R. Annapragada, D. Sun, S.V. Garimella, *Computational Materials Science* 40 (2007) 255–266.
- [89] G. Bonnet, *Journal of the Mechanics and Physics of Solids* 55 (2007) 881–899.
- [90] K. Honjo, *Carbon* 45 (2007) 865–872.
- [91] G.I. Giannopoulos, P.A. Kakavas, N.K. Anifantis, *Computational Materials Science* 41 (2008) 561–569.
- [92] M. Spies, *Materialprüfung* 42 (2000) 445–449.
- [93] D.L.S. McElwain, A.P. Roberts, A.H. Wilkins, *Acta Materialia* 54 (2006) 1995–2002.
- [94] R.M. Delvecchio, *IEEE Transactions on Magnetics* 16 (1980) 809–811.
- [95] M. Jackson, C. Stern, *Journal of Microwave Power and Electromagnetic Energy* 27 (1992) 103–111.
- [96] R. Kouddane, N. Zouhal, A. Molinari, G.R. Canova, *Materials Science and Engineering a—Structural Materials Properties Microstructure and Processing* 175 (1994) 31–36.
- [97] J. Paul, C. Christopoulos, D.W.P. Thomas, *Electromagnetics* 19 (1999) 527–546.
- [98] S. Iwata, N. Shichijo, T. Ashino, *Materials & Design* 22 (2001) 77–79.
- [99] C.P.E. Varsamis, *Applied Spectroscopy* 56 (2002) 1107–1113.
- [100] R.M. Walser, *Introduction to Complex Mediums for Electromagnetics and Optics*, SPIE Press, Bellingham, WA, USA, 2003.
- [101] K.C. Daoulas, M. Muller, M.P. Stoykovich, Y.J. Papakonstantopoulos, J.J. De Pablo, P.F. Nealey, S.M. Park, H.H. Solak, *Journal of Polymer Science Part B—Polymer Physics* 44 (2006) 2589–2604.
- [102] P. Trovati, *International Journal for Multiscale Computational Engineering* 5 (2007) VII–VIX.
- [103] W.Y. Ching, P. Rulis, *Physical Review B* 77 (2008) 035125.
- [104] A.C. Balazs, C. Singh, E. Zhulina, Y. Lyatskaya, *Accounts of Chemical Research* 32 (1999) 651–657.
- [105] Z.M. Huang, Y.Z. Zhang, M. Kotaki, S. Ramakrishna, *Composites Science and Technology* 63 (2003) 2223–2253.
- [106] V.A. Buryachenko, A. Roy, K. Lafdi, K.L. Anderson, S. Chellapilla, *Composites Science and Technology* 65 (2005) 2435–2465.
- [107] E.T. Thostenson, C.Y. Li, T.W. Chou, *Composites Science and Technology* 65 (2005) 491–516.
- [108] F. Hussain, M. Hojjati, M. Okamoto, R.E. Gorga, *Journal of Composite Materials* 40 (2006) 1511–1575.
- [109] Q.H. Zeng, A.B. Yu, G.Q. Lu, *Progress in Polymer Science* 33 (2008) 191–269.
- [110] J.C. Maxwell, *A Treatise on Electricity and Magnetism*, Clarendon Press, Oxford, 1873.
- [111] C.J.F. Bottcher, *Theory of Electric Polarization*, Elsevier, 1952.
- [112] R.W. Zimmerman, *Journal of Petroleum Science and Engineering* 3 (1989) 219–227.
- [113] W. Kreher, W. Pompe, *Internal Stresses in Heterogeneous Solids*, Akademie-Verlag, Berlin, 1989.
- [114] C.P. Wong, R.S. Bollampally, *Journal of Applied Polymer Science* 74 (1999) 3396–3403.
- [115] M. Orrhede, R. Tolani, K. Salama, *Research in Nondestructive Evaluation* 8 (1996) 23–37.
- [116] R. Landauer, *Journal of Applied Physics* 23 (1952) 779–784.
- [117] D.A.G. Bruggeman, *Annalen Der Physik* 24 (1935) 636–664.
- [118] D.A.G. Bruggeman, *Annalen Der Physik* 24 (1935) 665–679.
- [119] L. Gao, J.Z. Gu, *Journal of Physics D—Applied Physics* 35 (2002) 267–271.
- [120] Y. Rao, J.M. Qu, T. Marinis, C.P. Wong, *IEEE Transactions on Components and Packaging Technologies* 23 (2000) 680–683.
- [121] P.N. Sen, *Geophysics* 46 (1981) 1714–1720.
- [122] K.A. Snyder, E.J. Garboczi, A.R. Day, *Journal of Applied Physics* 72 (1992) 5948–5955.
- [123] J.C. Maxwell, *A treatise on Electricity and Magnetism*, Oxford University Press, Cambridge, UK, 1904.
- [124] A. Eucken, *Forschung Gabiete Ingenieur* 11 (1940) 6–20.
- [125] R.C. Landauer, in: J.C. Garland, D.B. Tanner (Eds.), *AIP Conference Proceedings*, vol. 2, New York, 1978.
- [126] D.S. McLachlan, *Journal of Physics C—Solid State Physics* 20 (1987) 865–877.
- [127] S.B. Jones, S.P. Friedman, *Water Resources Research* 36 (2000) 2821–2833.
- [128] R. Olives, S. Mauran, *Transport in Porous Media* 43 (2001) 377–394.
- [129] Y.M. Poon, F.G. Shin, *Journal of Materials Science* 39 (2004) 1277–1281.
- [130] D.A. Robinson, S.P. Friedman, *Water Resources Research* 37 (2001) 33–40.
- [131] B. Sareni, L. Krahenbuhl, A. Beroual, C. Brosseau, *Journal of Applied Physics* 80 (1996) 4560–4565.
- [132] B. Sareni, L. Krahenbuhl, C. Brosseau, *Journal of Applied Physics* 80 (1996) 1688–1696.
- [133] R.L. Hamilton, O.K. Crosser, *Industrial & Engineering Chemistry Fundamentals* 1 (1962) 187.
- [134] J.A. del Rio, R.W. Zimmerman, R.A. Dawe, *Solid State Communications* 106 (1998) 183–186.
- [135] J.B. Keller, *Journal of Mathematical Physics* 5 (1964) 548.
- [136] K.S. Mendelson, *Journal of Applied Physics* 46 (1975) 4740–4741.
- [137] C.W. Nan, R. Birringer, D.R. Clarke, H. Gleiter, *Journal of Applied Physics* 81 (1997) 6692–6699.
- [138] C.W. Nan, Z. Shi, Y. Lin, *Chemical Physics Letters* 375 (2003) 666–669.
- [139] M. Sahimi, G.R. Gavalas, T.T. Tsotsis, *Chemical Engineering Science* 45 (1990) 1443–1502.
- [140] K.J. Singh, R. Singh, D.R. Chaudhary, *Journal of Physics D—Applied Physics* 31 (1998) 1681–1687.
- [141] M.R.J. Wyllie, A.R. Gregory, *Petroleum Transactions AIME* 198 (1953) 103–110.
- [142] O. Krischer, *Die wissenschaftlichen Grundlagen der Trocknungstechnik (The Scientific Fundamentals of Drying Technology)*, Springer-Verlag, Berlin, 1963.
- [143] D.R. Chaudhary, R.C. Bhandari, *Journal of Physics D (British Journal of Applied Physics)* 1 (1968) 815–817.
- [144] T. Renaud, P. Briery, J. Andrieu, M. Laurent, *Journal of Food Engineering* 15 (1992) 83–97.
- [145] J.K. Carson, S.J. Lovatt, D.J. Tanner, A.C. Cleland, *International Journal of Heat and Mass Transfer* 48 (2005) 2150–2158.
- [146] J.F. Wang, J.K. Carson, M.F. North, D.J. Cleland, *International Journal of Heat and Mass Transfer* 49 (2006) 3075–3083.
- [147] Y. Agari, T. Uno, *Journal of Applied Polymer Science* 32 (1986) 5705–5712.
- [148] A. Bouguerra, *Journal of Physics D—Applied Physics* 32 (1999) 1407–1414.
- [149] P. Lehmann, M. Stahli, A. Papritz, A. Gygi, H. Fluhler, *Transport in Porous Media* 52 (2003) 313–332.
- [150] X.G. Liang, X. Ji, *International Journal of Heat and Mass Transfer* 43 (2000) 3633–3640.
- [151] X.G. Liang, W. Qu, *International Journal of Heat and Mass Transfer* 42 (1999) 1885–1893.
- [152] J.E.J. Staggs, *Fire Safety Journal* 37 (2002) 107–119.
- [153] B.M. Yu, B.W. Li, *Physical Review E* 73 (2006) 066302.
- [154] R.M. Christensen, *Mechanics of Composite Materials*, Krieger, Malabar, 1991.
- [155] S. Nemat-Nasser, M. Hori, *Micromechanics: Overall Properties of Heterogeneous Materials*, Elsevier/North-Holland, 1998.
- [156] Z. Hashin, S. Shtrikman, *Journal of Applied Physics* 33 (1962) 3125.
- [157] Z. Hashin, *Journal of Applied Mechanics—Transactions of the ASME* 50 (1983) 481–505.
- [158] Z. Hashin, S. Shtrikman, *Journal of the Mechanics and Physics of Solids* 11 (1963) 127–140.
- [159] R.W. Zimmerman, *Mechanics Research Communications* 19 (1992) 563–569.

- [160] R.A. Schapery, *Journal of Composite Materials* 2 (1968) 380.
- [161] A. Alharthi, J. Lange, *Water Resources Research* 23 (1987) 591–595.
- [162] G.K. Batchelor, R.W. Obrien, *Proceedings of the Royal Society of London Series A—Mathematical Physical and Engineering Sciences* 355 (1977) 313–333.
- [163] J.R. Birchak, C.G. Gardner, J.E. Hipp, J.M. Victor, *Proc. IEEE* 62 (1974) 93–98.
- [164] P. Cosenza, R. Guerin, A. Tabbagh, *European Journal of Soil Science* 54 (2003) 581–587.
- [165] S.P. Friedman, *Computers and Electronics in Agriculture* 46 (2005) 45–70.
- [166] M.T. Hallikainen, F.T. Ulaby, M.C. Dobson, M.A. Elrayes, L.K. Wu, *IEEE Transactions on Geoscience and Remote Sensing* 23 (1985) 25–34.
- [167] O.H. Jacobsen, P. Schjonning, *Journal of Hydrology* 151 (1993) 147–157.
- [168] S.B. Jones, D. Or, *Physica B—Condensed Matter* 338 (2003) 284–290.
- [169] T. Miyamoto, T. Annaka, J. Chikushi, *Vadose Zone Journal* 2 (2003) 90–97.
- [170] G.C. Topp, J.L. Davis, A.P. Annan, *Water Resources Research* 16 (1980) 574–582.
- [171] J.R. Wang, T.J. Schmugge, *IEEE Transactions on Geoscience and Remote Sensing* 18 (1980) 288–295.
- [172] W.R. Whalley, *Journal of Soil Science* 44 (1993) 1–9.
- [173] M. Chandrakanthi, A.K. Mehrotra, J.P.A. Hettiaratchi, *Environmental Pollution* 136 (2005) 167–174.
- [174] W. Woodside, J.H. Messmer, *Journal of Applied Physics* 32 (1961) 1688.
- [175] D.A.d. Veris, in: W.R.v. Wijk (Ed.), *Physics of Plant Environment*, North-Holland Publishing Company, Amsterdam, 1963, pp. 210–235.
- [176] G.P. Deloor, *Applied Scientific Research Section B—Electrophysics Acoustics Optics Mathematical Methods* 11 (1964) 310.
- [177] G.P.D. Looor, *The dielectric properties of wet soils*, The Netherlands Remote Sensing Board: bcrrs Rep. 90-13, 1990, pp. 1–39.
- [178] M.C. Dobson, F.T. Ulaby, M.T. Hallikainen, M.A. Elrayes, *IEEE Transactions on Geoscience and Remote Sensing* 23 (1985) 35–46.
- [179] S.P. Friedman, *Water Resources Research* 34 (1998) 2949–2961.
- [180] G. Dagan, *Flow and Transport in Porous Formations*, Springer-Verlag, New York, 1989.
- [181] W.R. Tinga, W.A.G. Voss, D.F. Blossey, *Journal of Applied Physics* 44 (1973) 3897–3902.
- [182] T. Miyamoto, T. Annaka, J. Chikushi, *Soil Science Society of America Journal* 69 (2005) 23–29.
- [183] F. Gori, S. Corasaniti, *International Journal of Thermophysics* 24 (2003) 1339–1353.
- [184] R. de Borst, *Computational Materials Science* 43 (2008) 1–15.
- [185] D. Raabe, *Modelling and Simulation in Materials Science and Engineering* 12 (2004) R13–R46.
- [186] N. Pan, *Journal of Composite Materials* 28 (1994) 1500–1531.
- [187] I.M. Young, J.W. Crawford, C. Rappoldt, *Soil & Tillage Research* 61 (2001) 33–45.
- [188] S. Wolfram, *A New Kind of Science*, Wolfram Media, Champaign, IL, 2002.
- [189] C.S. Du, D. Heldbrant, N. Pan, *Materials Letters* 57 (2002) 434–438.
- [190] C.S. Du, J. Yeh, N. Pan, *Journal of Materials Chemistry* 15 (2005) 548–550.
- [191] S. Torquato, I.C. Kim, D. Cule, *Journal of Applied Physics* 85 (1999) 1560–1571.
- [192] H.F. Zhang, X.S. Ge, H. Ye, *Journal of Physics D—Applied Physics* 39 (2006) 220–226.
- [193] L. Tacher, P. Perrochet, A. Parriaux, *Transport in Porous Media* 26 (1997) 99–107.
- [194] M. Pilotti, *Transport in Porous Media* 33 (1998) 257–278.
- [195] A. Yang, C.T. Miller, L.D. Torcoliver, *Physical Review E* 53 (1996) 1516–1524.
- [196] Y.S. Li, E.J. LeBoeuf, P.K. Basu, S. Mahadevan, *Advances in Water Resources* 28 (2005) 835–844.
- [197] Y. Mori, J.W. Hopmans, A.P. Mortensen, G.J. Kluitenberg, *Soil Science Society of America Journal* 69 (2005) 599–606.
- [198] A.P. Mortensen, J.W. Hopmans, Y. Mori, J. Simunek, *Advances in Water Resources* 29 (2006) 250–267.
- [199] D.S. Li, G. Saheli, M. Khaleel, H. Garmestani, *Computational Materials Science* 38 (2006) 45–50.
- [200] K. Makrodimitris, G.K. Papadopoulos, C. Philippopoulos, D.N. Theodorou, *Journal of Chemical Physics* 117 (2002) 5876–5884.
- [201] N. Losic, J.F. Thovort, P.M. Adler, *Journal of Colloid and Interface Science* 186 (1997) 420–433.
- [202] S. Torquato, *International Journal of Solids and Structures* 37 (2000) 411–422.
- [203] A.R. Dexter, *Journal of Soil Science* 27 (1976) 267–278.
- [204] K.J. Wu, N. Nunan, J.W. Crawford, I.M. Young, K. Ritz, *Soil Science Society of America Journal* 68 (2004) 346–351.
- [205] S. Torquato, *Annual Review of Materials Research* 32 (2002) 77–111.
- [206] P.M. Adler, *Porous Media: Geometry and Transports*, Butterworth/Heinemann, Stoneham, 1992.
- [207] S. Torquato, *Random Heterogeneous Materials: Microstructure and Macroscopic Properties*, Springer, New York, 2002.
- [208] N. Pan, P. Gibson (Eds.), *Thermal and Moisture Transport in Fibrous Material*, Woodhead Publishing Ltd, Cambridge, UK, 2006.
- [209] X.J. Hu, J.H. Du, S.Y. Lei, B.X. Wang, *International Journal of Heat and Mass Transfer* 44 (2001) 247–251.
- [210] M. Kohout, A.P. Collier, F. Stepanek, *International Journal of Heat and Mass Transfer* 47 (2004) 5565–5574.
- [211] S. Mohanty, *Journal of Physics D—Applied Physics* 30 (1997) L80–L84.
- [212] P. Meakin, *Fractals, Scaling and Growth Far from Equilibrium*, Cambridge University Press, Cambridge, 1998.
- [213] M.R. Wang, N. Pan, J.K. Wang, S.Y. Chen, *Journal of Colloid and Interface Science* 311 (2007) 562–570.
- [214] M.R. Wang, J.H. He, J.Y. Yu, N. Pan, *International Journal of Thermal Sciences* 46 (2007) 848–855.
- [215] M. Wang, N. Pan, *Applied Thermal Engineering*, 10.1016/j.applthermaleng.2008.03.004.
- [216] M. Wang, N. Pan, *International Journal of Heat and Mass Transfer* 51 (2008) 1325–1331.
- [217] X.Y. He, L.S. Luo, *Physical Review E* 55 (1997) R6333–R6336.
- [218] M. Wang, S. Chen, *Journal of Colloid and Interface Science* 314 (2007) 264–273.
- [219] S.J. Eichhorn, W.W. Sampson, *Journal of the Royal Society Interface* 2 (2005) 309–318.
- [220] K. Boomsma, D. Poulikakos, *International Journal of Heat and Mass Transfer* 44 (2001) 827–836.
- [221] J.F. Thovort, F. Wary, P.M. Adler, *Journal of Applied Physics* 68 (1990) 3872–3883.
- [222] D. Coelho, J.F. Thovort, P.M. Adler, *Physical Review E* 55 (1997) 1959–1978.
- [223] K. Bakker, *International Journal of Heat and Mass Transfer* 40 (1997) 3503–3511.
- [224] A.G. Fedorov, R. Viskanta, *International Journal of Heat and Mass Transfer* 43 (2000) 399–415.
- [225] A. Horvat, I. Catton, *International Journal of Heat and Mass Transfer* 46 (2003) 2155–2168.
- [226] A. Sutradhar, G.H. Paulino, *Computer Methods in Applied Mechanics and Engineering* 193 (2004) 4511–4539.
- [227] H.F. Zhang, X.S. Ge, H. Ye, *Modelling and Simulation in Materials Science and Engineering* 13 (2005) 401–412.
- [228] K. Karkkainen, A. Sihvola, K. Nikoskinen, *IEEE Transactions on Geoscience and Remote Sensing* 39 (2001) 1013–1018.
- [229] K. Asami, *Journal of Colloid and Interface Science* 292 (2005) 228–235.
- [230] K. Asami, *Journal of Physics D—Applied Physics* 39 (2006) 492–499.
- [231] E. Tuncer, S.M. Gubanski, B. Nettelblad, *Journal of Applied Physics* 89 (2001) 8092–8100.
- [232] I. Krakovsky, V. Myroshnychenko, *Journal of Applied Physics* 92 (2002) 6743–6748.
- [233] A. Mejdoubi, C. Brosseau, *Journal of Applied Physics* 100 (2006) 094103.
- [234] K. Sekine, C. Kuroda, N. Torii, *Colloid and Polymer Science* 280 (2002) 71–77.
- [235] K. Sekine, Y. Watanabe, S. Hara, K. Asami, *Biochimica Et Biophysica Acta—General Subjects* 1721 (2005) 130–138.
- [236] J.P. Calame, *Journal of Applied Physics* 99 (2006) 2188032.
- [237] V. Myroshnychenko, C. Brosseau, *Physical Review E* 71 (2005) 016701.
- [238] D.X. Zhang, *Stochastic Method for Flow in Porous Media*, Academic Press, London, 2002.
- [239] D. Kulasiri, W. Verwoerd, *Stochastic Dynamics Modeling Solute Transport in Porous Media*, Elsevier, New York, 2002.
- [240] Y. Shoshany, D. Prialnik, M. Podolak, *ICARUS* 157 (2002) 219–227.
- [241] S. Barta, P. Dieska, *Kovove Materialy—Metallic Materials* 40 (2002) 99–112.
- [242] W.Z. Yue, G. Tao, K.Q. Zhu, *Chinese Journal of Geophysics—Chinese Edition* 47 (2004) 905–910.
- [243] W.Z. Yue, G. Tao, K.Q. Zhu, *Chinese Journal of Geophysics—Chinese Edition* 48 (2005) 189–195.
- [244] Q.J. Kang, D.X. Zhang, S.Y. Chen, X.Y. He, *Physical Review E* 65 (2002) 036318.
- [245] Q.J. Kang, D.X. Zhang, S.Y. Chen, *Journal of Geophysical Research—Solid Earth* 108 (2003) 2505.
- [246] D.X. Zhang, Q.J. Kang, *Geophysical Research Letters* 31 (2004) L12504.
- [247] Q.J. Kang, P.C. Lichtner, D.X. Zhang, *Journal of Geophysical Research—Solid Earth* 111 (2006) B05203.
- [248] M. Wang, N. Pan, J.K. Wang, S.Y. Chen, *Communications in Computational Physics* 2 (2007) 1055–1070.
- [249] M. Wang, J.K. Wang, S.Y. Chen, N. Pan, *Journal of Colloid and Interface Science* 304 (2006) 246–253.
- [250] E.K. Muhammed, H.A. Ahmet, M. Eyad, *Computers and Geotechnics* 33 (2006) 381–395.
- [251] S. Chen, G.D. Doolen, *Annual Review of Fluid Mechanics* 30 (1998) 329–364.
- [252] S. Succi, *The Lattice Boltzmann Equation for Fluid Dynamics and Beyond*, Oxford Science Press, London, 2001.
- [253] J.K. Wang, *Lattice Boltzmann Simulation on Heat Transfer and Electro-Osmotic Flow in Micro Channel*, Department of Engineering Mechanics, Tsinghua University, Beijing, China, 2006.
- [254] J. Wang, M. Wang, Z. Li, *Communications in Nonlinear Science and Numerical Simulation* 13 (2008) 575–583.
- [255] X.Y. He, S.Y. Chen, R.Y. Zhang, *Journal of Computational Physics* 152 (1999) 642–663.
- [256] J.K. Wang, M. Wang, Z.X. Li, *International Journal of Thermal Sciences* 46 (2007) 228–234.
- [257] Y. Peng, C. Shu, Y.T. Chew, *Physical Review E* 68 (2003) 026701.
- [258] X.Y. He, N. Li, *Computer Physics Communications* 129 (2000) 158–166.
- [259] C.Y. Chan, R.J. Knight, *Water Resources Research* 37 (2001) 1099–1105.
- [260] X. Chen, P. Han, *International Journal of Heat and Fluid Flow* 21 (2000) 463–467.
- [261] V. Myroshnychenko, C. Brosseau, *Journal of Applied Physics* 97 (2005) 044101.
- [262] J.Y. Qian, Q. Li, K. Yu, Y.M. Xuan, *Science in China Series E—Technological Sciences* 47 (2004) 716–724.
- [263] C.R. Wylie, L.C. Barrett, *Advanced Engineering Mathematics*, McGraw-Hill Book Company, New York, 1982.
- [264] E.J. Garboczi, A.R. Day, *Journal of the Mechanics and Physics of Solids* 43 (1995) 1349–1362.
- [265] M. Wang, N. Pan, *Journal of Computational Physics*, in review.
- [266] G.D. Doolen, *Lattice Gas Methods for Partial Differential Equations*, Addison Wesley, New York, 1990.
- [267] Y.H. Qian, D. Dhumieres, P. Lallemand, *Europhysics Letters* 17 (1992) 479–484.

- [268] A. D'Orazio, S. Succi, *Computational Science—ICCS 2003, Pt I Proceedings* 2657 (2003) 977–986.
- [269] Q.S. Zou, X.Y. He, *Physics of Fluids* 9 (1997) 1591–1598.
- [270] H.J. Lee, R.E. Taylor, *Journal of Applied Physics* 47 (1976) 148–151.
- [271] A.K. Singh, R. Singh, D.R. Chaudhary, *Journal of Physics D—Applied Physics* 23 (1990) 698–702.
- [272] S. Fukusako, *International Journal of Thermophysics* 11 (1990) 353–372.
- [273] A.R. Sepaskhah, L. Boersma, *Soil Science Society of America Journal* 43 (1979) 439–444.
- [274] R. Prasher, W. Evans, P. Meakin, J. Fish, P. Phelan, P. Keblinski, *Applied Physics Letters* 89 (2006).
- [275] J. Eapen, J. Li, S. Yip, *Physical Review Letters* 98 (2007) 028302.
- [276] T.Y. Chen, G.J. Weng, W.C. Liu, *Journal of Applied Physics* 97 (2005) 1896094.
- [277] R. Singh, H.S. Kasana, *Applied Thermal Engineering* 24 (2004) 1841–1849.
- [278] <http://foam-materials.globalspec.com/>.
- [279] H.M. Yin, G.H. Paulino, W.G. Buttler, L.Z. Sun, *Journal of Applied Physics* 98 (2005) 2039998.
- [280] P.N. Sen, C. Scala, M.H. Cohen, *Geophysics* 46 (1981) 781–795.
- [281] M. Persson, B. Sivakumar, R. Berndtsson, O.H. Jacobsen, P. Schjonning, *Soil Science Society of America Journal* 66 (2002) 1424–1429.
- [282] J.M. Blonquist, S.B. Jones, I. Lebron, D.A. Robinson, *Water Resources Research* 42 (2006) 004418.
- [283] M.T. Tilbrook, R. Moon, M. Hoffman, *Materials Science and Engineering A—Structural Materials Properties Microstructure and Processing* 393 (2005) 170–178.
- [284] N. Pan, R. Postle, *Philosophical Transactions of the Royal Society of London Series A—Mathematical Physical and Engineering Sciences* 354 (1996) 1875–1897.
- [285] N. Pan, S.M. Zhao, T. Hua, *Polymer Composites* 21 (2000) 187–195.
- [286] K. Middtomme, E. Roaldset, *Petroleum Geoscience* 4 (1998) 165–172.
- [287] M.S. Majdoub, P. Sharma, T. Cagin, *Physical Review B* 77 (2008) 125424.
- [288] G.N. Dulnev, D.P. Volkov, A.B. Utkin, *Journal of Engineering Physics and Thermophysics* 52 (1987) 213–217.
- [289] V.V. Polyakov, M.A. Utemesov, A.V. Egorov, *Journal of Engineering Physics and Thermophysics* 68 (1995) 580–583.
- [290] J.Z. Liang, F.H. Li, *Polymer Testing* 25 (2006) 527–531.
- [291] X.G. Cheng, Z.X. Li, Z.Y. Guo, *Science in China Series E—Technological Sciences* 46 (2003) 296–302.
- [292] Z.Y. Guo, H.Y. Zhu, X.G. Liang, *International Journal of Heat and Mass Transfer* 50 (2007) 2545–2556.
- [293] H.S. Tekce, D. Kumlutas, I.H. Tavman, *Journal of Reinforced Plastics and Composites* 26 (2007) 113–121.
- [294] J.K. Carson, S.J. Lovatt, D.J. Tanner, A.C. Cleland, *Journal of Food Engineering* 63 (2004) 87–95.
- [295] Y.P. Xi, K. William, D.M. Frangopol, *Journal of Engineering Mechanics—ASCE* 126 (2000) 258–265.
- [296] W.A. Goddard, T. Cagin, M. Blanco, N. Vaidehi, S. Dasgupta, W. Floriano, M. Belmares, J. Kua, G. Zamanakos, S. Kashiwara, M. Iotov, G.H. Gao, *Computational and Theoretical Polymer Science* 11 (2001) 329–343.
- [297] T. Cagin, G.F. Wang, R. Martin, G. Zamanakos, N. Vaidehi, D.T. Mainz, W.A. Goddard, *Computational and Theoretical Polymer Science* 11 (2001) 345–356.
- [298] N.S. Martys, J.G. Hagedorn, *Materials and Structures* 35 (2002) 650–658.
- [299] N.M. Ghoniem, K. Cho, *CMES—Computer Modeling in Engineering & Sciences* 3 (2002) 147–173.
- [300] K. Caspersen, A. Lew, M. Ortiz, E.A. Carter, *Abstracts of Papers of the American Chemical Society* 225 (2003) U519–U519.
- [301] L. Stainier, A.M. Cuitino, M. Ortiz, *Journal De Physique IV* 105 (2003) 157–164.
- [302] S. Sinha, K.E. Goodson, *International Journal for Multiscale Computational Engineering* 3 (2005) 107–133.
- [303] K. Lebedev, S. Mafe, P. Stroeve, *Journal of Physical Chemistry B* 109 (2005) 14523–14528.
- [304] V.A.B. Narayanan, N. Zabaras, *Journal of Computational Physics* 202 (2005) 94–133.
- [305] S. Pricl, M. Ferrone, M. Fermiglia, F. Amato, C. Cosentino, M.M.C. Cheng, R. Walczak, M. Ferrari, *Biomedical Microdevices* 8 (2006) 277–290.
- [306] F. Amato, C. Cosentino, S. Pricl, M. Ferrone, M. Fermiglia, M.M.C. Cheng, R. Walczak, M. Ferrari, *Biomedical Microdevices* 8 (2006) 291–298.
- [307] S.E. Albo, L.J. Broadbelt, R.Q. Snurr, *AIChE Journal* 52 (2006) 3679–3687.
- [308] J.B. Bassingthwaight, H.J. Chizeck, L.E. Atlas, *Proceedings of the IEEE* 94 (2006) 819–831.
- [309] G.E. Kapellos, T.S. Alexiou, A.C. Payatakes, *Mathematical Biosciences* 210 (2007) 177–237.
- [310] J.W. Garvin, Y. Yang, H.S. Udaykumar, *International Journal of Heat and Mass Transfer* 50 (2007) 2952–2968.
- [311] S. Conti, P. Hauret, M. Ortiz, *Multiscale Modeling & Simulation* 6 (2007) 135–157.
- [312] G. Csanyi, G. Moras, J.R. Kermode, M.C. Payne, A. Mainwood, A. De Vita, *Theory of Defects in Semiconductors*, vol. 104, 2007, pp. 193–212.
- [313] Y. Xu, N.R. Aluru, *Physical Review B* 77 (2008) 075313.
- [314] H.F. Zhang, X.S. Ge, H. Ye, *Applied Physics Letters* 89 (2006).
- [315] C.S. Pande, A.K. Rajagopal, S. Abe, *Indo-US Workshop on “Nanoscale materials: From Science to Technology”*, Puri, India, 2004.
- [316] Z. Li, C. Lim, L. He, *European Journal of Mechanics, A/Solids* 25 (2006) 260–270.
- [317] K.K. Nanda, A. Maisels, F.E. Kruijs, H. Fissan, S. Stappert, *Physical Review Letters* 91 (2003) 106102.
- [318] T. Shinohara, T. Sato, T. Taniyama, *Physical Review Letters* 91 (2003) 197201.
- [319] H.J. Mamin, R. Budakian, B.W. Chui, D. Rugar, *Physical Review Letters* 91 (2003) 207604.
- [320] R.A. Masumura, P.M. Hazzledine, C.S. Pande, *Acta Materialia* 46 (1998) 4527–4534.
- [321] J.C.M. Li (Ed.), *Microstructure and Properties of Materials*, World Scientific, Singapore, 1996.
- [322] H. Kachkachi, D.A. Garanin, *Magnetic Nanoparticles as Many-Spin Systems, Surface Effects in Magnetic Nanoparticles*. Ed. D. Fiorani, *Nanostructure Science and Technology*, Ed. D. J. Lockwood, Springer, US, Pages 75–104, 2005.
- [323] D. Gerion, A. Hirt, A. Chatelain, *Physical Review Letters* 83 (1999) 532–535.
- [324] C. Goldenberg, I. Goldhirsch, *Physical Review Letters* 89 (2002) 084302.
- [325] P. Sharma, L.T. Wheeler, *Journal of Applied Mechanics* 74 (2007) 447–454.
- [326] M. Hartmann, G. Mahler, O. Hess, *Fundamentals of Nano-Thermodynamics*, in: Michael Rieth, Wolfram Schommers (Eds.), *Handbook of Theoretical and Computational Nanotechnology*, American Scientific Publishers, 2007.
- [327] D.S. Dean, A. Lefevre, *Physical Review Letters* 90 (2003) 198301.
- [328] S. Abe, A.K. Rajagopal, *Nanothermodynamics—A general approach to material properties at nanoscale*, in: S.N. Sahu, R.K. Choudhury, P. Jena (Eds.), *Nano-Scale Materials*, Nova Science Publishers, Inc, 2006, pp. 241–248.
- [329] E.M. Conwell, *Effect of Negative Differential Conductance in Carbon Nanotubes*, *Nano Lett.* 8 (4) (2008) 1253–1256.
- [330] A.A. Balandin, S. Ghosh, W.Z. Bao, I. Calizo, D. Teweldebrhan, F. Miao, C.N. Lau, *Nano Letters* 8 (2008) 902–907.
- [331] N.C. Mainak Majumder, Rodney Andrews, Bruce J. Hinds, *Nature* 438 (2005) 44.
- [332] W. Zhong, N. Pan, D. Lukas, *Journal of Computational and Theoretical Nanoscience* 3 (2006) 506–512.
- [333] J.P. Crocombette, G. Dumazer, N.Q. Hoang, F. Gao, W.J. Weber, *Journal of Applied Physics* 101 (2007) 023527.
- [334] S. Leonard, P. Mayer, P. Sollich, L. Berthier, J.P. Garrahan, *Journal of Statistical Mechanics—Theory and Experiment* (2007).
- [335] J.F. VelezRuiz, G.V.B. Canovas, *Critical Reviews in Food Science and Nutrition* 37 (1997) 311–359.
- [336] J.K.C. Suen, Y.L. Joo, R.C. Armstrong, *Annual Review of Fluid Mechanics* 34 (2002) 417–444.
- [337] P.G. De Gennes, *Soft Matter: Nobel Lecture*, in: *Nobel Lectures, Physics vol. 1991–1995*, World Scientific Publishing, Singapore, 1991.
- [338] N. Pan, J.H. He, J.Y. Yu, *Textile Research Journal* 77 (2007) 205–213.
- [339] D. Bruno, S. Lato, R. Zinno, *Composites Engineering* 3 (1993) 419–435.
- [340] W.W. Eltahan, G.H. Staab, S.H. Advani, J.K. Lee, *Journal of Engineering Mechanics—ASCE* 115 (1989) 963–981.
- [341] E. Sacco, J.N. Reddy, *Journal of Applied Mechanics—Transactions of the ASME* 59 (1992) 220–221.
- [342] N. Pan, D. Brookstein, *Journal of Applied Polymer Science* 83 (2002) 610–630.
- [343] R.W. Zimmerman, *Compressibility of Sandstones*, Elsevier Science Pub. Co, New York, 1991.
- [344] N.W. Tschoegl, W.G. Knauss, I. Emri, *Mechanics of Time-Dependent Materials* 6 (2002) 3–51.
- [345] H.Y. Sun, N. Pan, R. Postle, *Composite Structures* 68 (2005) 505–510.
- [346] H. Gercek, *International Journal of Rock Mechanics and Mining Sciences* 44 (2007) 1–13.
- [347] J. Ophir, S.K. Alam, B. Garra, F. Kallel, E. Konofagou, T. Krouskop, T. Varghese, *Proceedings of the Institution of Mechanical Engineers Part H—Journal of Engineering in Medicine* 213 (1999) 203–233.
- [348] T. Rouxel, *Comptes Rendus Mecanique* 334 (2006) 743–753.
- [349] B. Erman, *Superabsorbent Polymers*, vol. 573, 1994, pp. 50–63.
- [350] T.L. Sun, L. Feng, X.F. Gao, L. Jiang, *Accounts of Chemical Research* 38 (2005) 644–652.
- [351] M.L. Ma, R.M. Hill, *Current Opinion in Colloid & Interface Science* 11 (2006) 193–202.
- [352] P. Roach, N.J. Shirtcliffe, M.I. Newton, *Soft Matter* 4 (2008) 224–240.
- [353] W.R. Hansen, K. Autumn, *Proceedings of the National Academy of Sciences of the United States of America* 102 (2005) 385–389.
- [354] P. Gould, *Nano Today* 2 (2007) 12.
- [355] S. Sethi, L. Ge, L. Ci, P.M. Ajayan, A. Dhinojwala, *Nano Letters* 8 (2008) 822–825.
- [356] H. Tabata, K. Kumazawa, M. Funakawa, J. Takimoto, M. Akimoto, *Optical Review* 3 (1996) 139–145.
- [357] H.F. Nijhout, *Journal of Experimental Zoology* 291 (2001) 213–225.
- [358] D.G. Stavenga, K. Arikawa, *Arthropod Structure & Development* 35 (2006) 307–318.
- [359] S. Banerjee, Z. Dong, *Optical Review* 14 (2007) 359–361.
- [360] M.W. Feise, J.B. Schneider, P.J. Bevelacqua, *IEEE Transactions on Antennas and Propagation* 52 (2004) 2955–2962.
- [361] J. Manzanares-Martinez, J. Gaspar-Armenta, *Journal of Electromagnetic Waves and Applications* 21 (2007) 2297–2310.
- [362] C.G. Du, H.Y. Chen, S.Q. Li, *Physical Review B* 74 (2006) 113105.
- [363] A.O. Cakmak, K. Guven, E. Ozbay, *Physica Status Solidi B—Basic Solid State Physics* 244 (2007) 1188–1191.
- [364] M. Antonietti, *Nature Materials* 2 (2003) 9–10.
- [365] M.J. Buehler, *Journal of Computational and Theoretical Nanoscience* 3 (2006) 603–623.
- [366] S. Sass, *Substance of Civilization: Materials Human History from the Stone Age to Age of Silicon*, Arcade Publishing, New York, 1998.
- [367] S. Srinivasan, S. Ranganathan, *Transactions of the Indian Institute of Metals* 59 (2006) 829–846.